The orientation of polymers to produce high performance materials

Recent research at Leeds University has shown that the physical properties of polymers can be improved dramatically by stretching processes whose principal aim is to produce a high degree of molecular orientation. In polyethylene and a few other polymers, very high degrees of stretch have led to spectacular improvements in stiffness and strength.

In polyethylene, particular attention has been given to the creep behaviour under sustained load. Guidelines have been established for the sensitivity of the creep behaviour to such variables as polymer molecular weight, degree of copolymerisation and draw ratio. With this information, it is possible to optimise the situation with regard to the possibility of ultimate failure.

I. M. Ward, *University of Leeds*

INTRODUCTION

The discovery of methods for the preparation of ultra high modulus polyethylene by tensile drawing to very high draw ratios[1] raised the possibility that such materials might be used for the reinforcement of brittle matrices such as cement[2], concrete[3] or polymeric resins[4]. This requires that the oriented polymer should be subjected to continuous loading without this leading to failure. During recent years extensive studies of the creep and recovery behaviour of oriented polyethylene[5] and polypropylene[6] have been carried out at Leeds University. The aim of the work was two fold (1) to establish criteria for creep failure (2) to identify structural factors which lead to improvement in creep performance. The results of these studies have been of direct relevance to Tensar and have provided guidelines for the development of Tensar for engineering applications.

THE PRODUCTION AND PROPERTIES OF DRAWN POLYETHYLENE

The discovery of high modulus polyethylene stemmed from the recognition that the Young's modulus of fibres and tapes produced by tensile drawing relates to the draw ratio, and increases steadily with increasing draw ratio[1]. The limitation of a natural draw ratio was replaced by the concept of effective drawing i.e. drawing at a temperature and strain rate which avoids fracture on the one hand, and "flow drawing" where the molecules relax to isotropy, on the other.

It is therefore useful to consider the properties of oriented polymers in terms of the draw ratio as a key variable, alongside other variables such as molecular weight, molecular weight distribution, and degree of branching or cross-linking. Fig. 1 shows the creep compliance (extensional strain/applied stress) for linear polyethylene (Rigidex 50 grade) of draw ratios $\lambda = 10$ and 30, each sample being measured at three levels of stress. It can be seen that there is a marked reduction in creep compliance with draw ratio. Although in all cases the creep compliance is not independent of stress level (the behaviour is non-linear) the response is more nearly linear at the highest draw ratio.

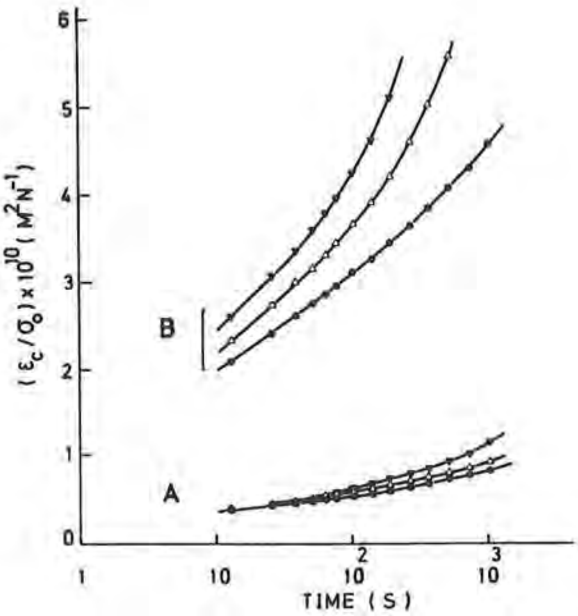

Fig.1. Creep compliance (ε_c/σ_o) of drawn Rigidex 50 samples A, λ=30 and C, λ=10 at 0.1 (•), 0.15 (Δ) and 0.2 GPa (▼) applied stress σ_o as a function of time. (Reproduced from Polymer 19, 969 (1978) by permission of the publishers, Butterworth & Co. (Publishers) Ltd. (C).

Although Fig. 1 shows the effect of draw ratio on the creep behaviour, it is not so revealing as the plots of creep rate versus total creep strain. Sherby and Dorn[6] used such plots to represent their data for the creep of isotropic polymethylmethacrylate (PMMA). This was because they adopted the approach of considering that the total creep behaviour can be represented by a thermally activated process, so that it should be possible to construct a master curve for data over a range of temperatures. Although the case of oriented polyethylene is not quite as tractable as PMMA, we have

Polymer grid reinforcement. Thomas Telford Limited, London, 1985

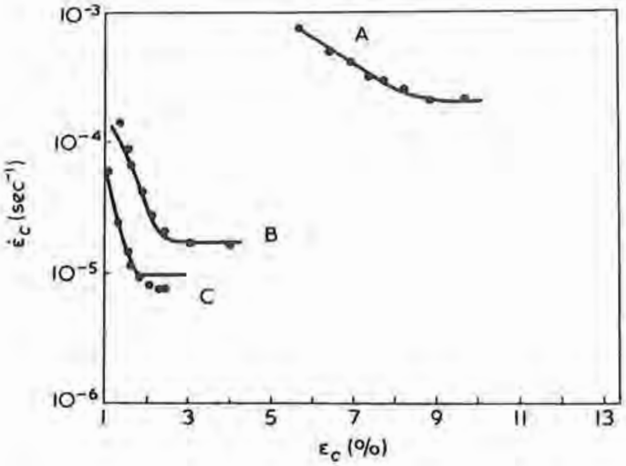

Fig.2. Creep strain rate $\dot{\varepsilon}_c$ as a function of ε_c at 0.2 GPa applied stress for drawn Rigidex 50 samples A, λ=10, B, λ=20, C, λ=30. (Reproduced from Polymer 19, 969 (1978) by permission of the publishers, Butterworth & Co. (Publishers) Ltd. (C).

used "Sherby-Dorn Plots" to describe the results to some advantage.

Fig.2 shows these plots for the same samples as those described by Fig. 1. In contrast to Sherby and Dorn's results, the creep rates fall to a constant rate which is independent of strain and it was established that there was no simplistic stress/temperature superposition rule for the plots as a whole. However, the constant creep rates (which we have termed the plateau creep rates $\dot{\varepsilon}_p$) were shown to depend on stress σ and temperature T is a manner expected for a single thermally activated process, leading to the so-called Eyring equation

$$\dot{\varepsilon}_p = \dot{\varepsilon}_o \exp - \frac{\Delta H}{kT} \sinh \frac{\sigma v}{kT} \quad (1)$$

where ΔH, v are the activation energy and activation volume respectively, $\dot{\varepsilon}_o$ is a constant pre-exponential factor and k is Boltzmann's constant.

It was concluded that there is an initial viscoelastic region, where the creep rate falls with time (and hence creep strain) followed by a second region where the creep rate is constant, and corresponds to a permanent flow plastic deformation process which is irrecoverable and will eventually lead to failure of the sample.

This is the behaviour of the first sample of oriented polyethylene to be examined, a linear polymer of low molecular weight. It could be very well modelled by the arrangement of springs and dashpots shown in Fig.3(b), which is essentially a linear Voigt element in series with a Maxwell element which contains an Eyring dashpot. Materials of this kind would be unsuitable for load-bearing applications as there will always be an element of permanent plastic deformation, even at very low stresses, which could lead to failure, albeit at very long times.

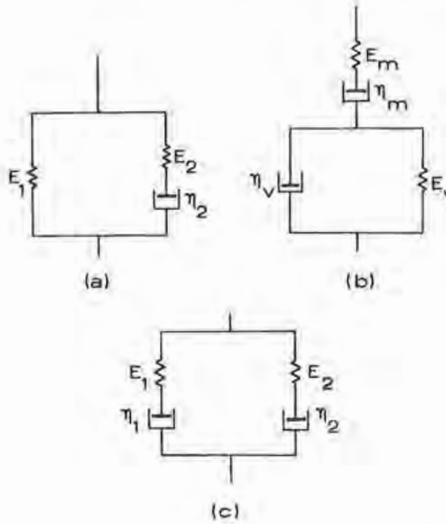

Fig.3. Schematic representation of the four element mechanical model for creep and recovery. (Reproduced from Polymer 22, 870 (1981) by permission of the publishers, Butterworth & Co. (Publishers) Ltd. (C).

It was therefore considered essential to produce oriented polyethylenes of greatly improved creep response esponse, and this has been achieved in three ways

(1) by increasing molecular weight
(2) by cross-linking the polymer
(3) by use of copolymers.

Details of samples studied are given in Table 1.

Table 1.

Sample details

Polymer Grade†	$\bar{M}_n$	$\bar{M}_w$	Chemical Composition
Rigidex 50	6,180	101,450	Homopolymer
Rigidex 006-60	6,000	130,000	Homopolymer
Rigidex HO20-54P	33,000	312,000	Homopolymer
Rigidex 002-55	16,900	155,000	Ethylene/Hexene Copolymer ca 1.5 butyl/ 10^3 carbon atoms
Rigidex 50	6,180	101,450	Homopolymer γ-irradiated (2Mr) before drawing

† BP Chemicals International Ltd.

In Fig. 4, Sherby-Dorn plots for a higher molecular weight polyethylene homopolymer are compared with those for the lower molecular weight material shown in Figs. 1 and 2. It can be seen that at the lowest stress level, the Sherby-Dorn plot for the higher molecular weight polymer shows a continuously decreasing strain-rate with increasing strain. This implies that at low stress levels this material reaches an equilibrium

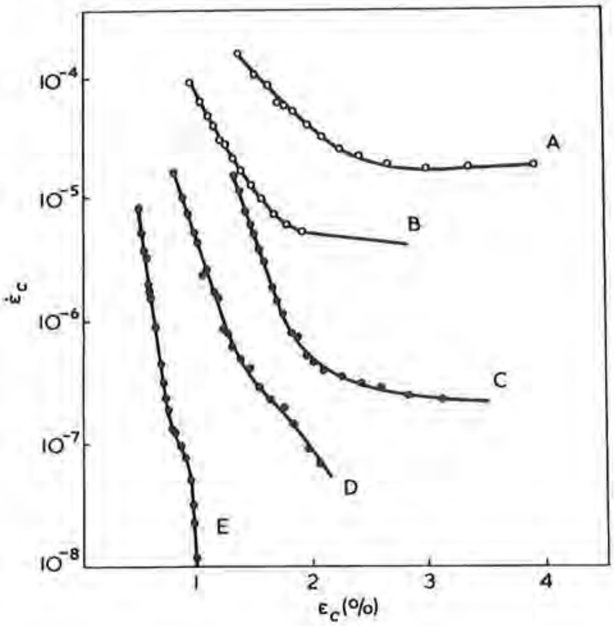

Fig. 4. Creep strain rate $\dot{\varepsilon}_c$ as a function of strain for Rigidex 50, λ=20 (o) ($\bar{M}_w \sim$ 100,000) and Rigidex H020, λ=20 (●) ($\bar{M}_w \sim$ 300,000) A, 0.2; B, 0.15; C, 0.2; D, 0.15, E, 0.1 GPa. (Reproduced from Polymer 19, 969 (1978) by permission of the publishers, Butterworth & Co. (Publishers) Ltd. (C)).

strain, as shown in Fig. 5, so that failure does not occur. In practical terms, this means that there is a

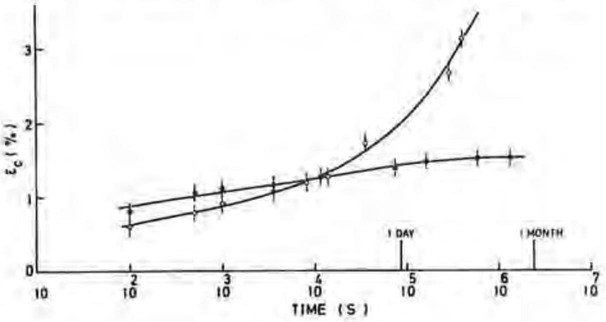

Fig.5. A comparison of the long term creep response of Rigidex 50, λ=20 (o) and Rigidex H020, λ=20 (●) at 0.1 GPa applied stress (——) are visual fits and the error bars correspond to the accuracy of the measurements. (Reproduced from Polymer 19, 969 (1978) by permission of the publishers, Butterworth & Co.(Publishers) Ltd. (C).

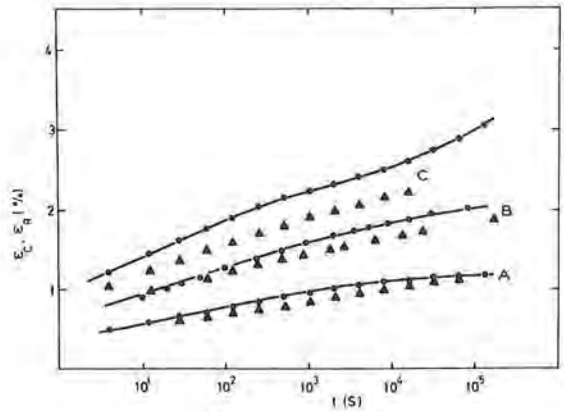

Fig. 6. Creep ε_c and recovery ε_R curves for Rigidex 002-55 copolymer, λ=20 ($\bar{M}_w$ = 155,000, ca 1.5 butyl branches per 10^3 carbon atoms) (●) creep (▲) recovery. A, 0.1 GPa, B, 0.15 GPa, C, 0.2 GPa. (Reproduced from Polymer 22, 870 (1981) by permission of the publisher, Butterworth & Co. (Publishers) Ltd. (C)).

safe critical stress level for long term loading. In Fig. 6, similar results are shown for a copolymer, and it can be seen that the presence of a very small number of side branches ($\sim$ 1 per 1,000 carbon atoms) is extremely effective in altering the creep behaviour.

The concept of a critical stress for permanent flow creep, although valuable for engineering design is somewhat obscure in terms of polymer physics. It is therefore necessary to pursue the analysis of the data further to bring the behaviour within the general scheme of our present understanding of deformation processes in polymers.

It has been proposed that a more appropriate first-order representation for the viscoelastic behaviour of these materials is by two Maxwell elements in parallel, the two dashpots each corresponding to thermally activated processes, (Figure 3(c)). The equilibrium creep behaviour is then described by the situation where the two springs have reached their equilibrium extension and the total creep rate is constant, with the stress divided across the two dashpots. If the two thermally activated dashpots are very different in kind, one having a large activation volume v_1 and the other a small activation volume v_2, we have

$$\frac{\sigma}{T} = \frac{k}{v_1}\left[\frac{\Delta H_1}{kT} + \ln \frac{2\dot{\varepsilon}_p}{[\dot{\varepsilon}_o]_1}\right] + \frac{k}{v_2}\sinh^{-1}\left[\frac{\dot{\varepsilon}_p}{[\dot{\varepsilon}_o]}\exp\frac{\Delta H_2}{kT}\right] \quad (2)$$

where the two activated processes are denoted by the subscript symbols 1 and 2 respectively. σ is the applied tensile stress at a temperature T^oK, $\dot{\varepsilon}_p$ the creep rate, $[\dot{\varepsilon}_o]$ the pre-exponential factor, ΔH the activation energy and k is Boltzmann's constant.

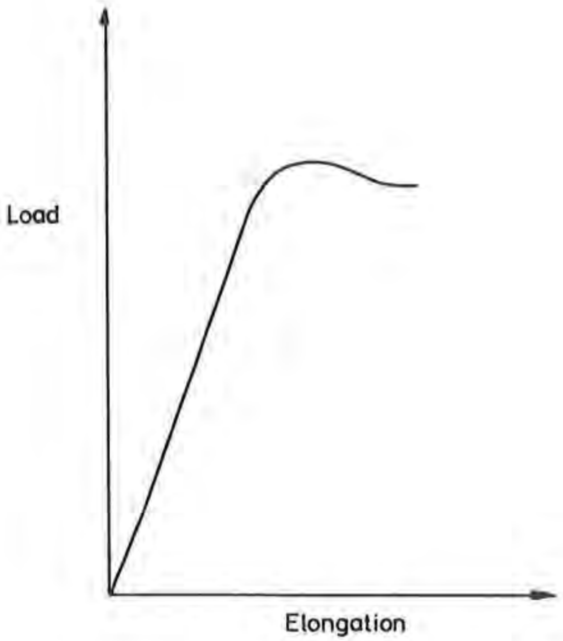

Fig. 7. The yield point in a constant strain rate test.

This representation is familiar to polymer scientists in respect of the yield behaviour of isotropic polymers[7,8]. In general, a yield point is observed in a constant strain rate test (Figure 7). The point of maximum load represents the point at which the plastic flow rate $\dot{\varepsilon}_p$ matches the imposed strain rate of the testing machine. The relationship between the maximum stress (the yield or flow stress) and the imposed strain rate can generally be represented by equation (2), as shown in Fig. 8(a). In Fig. 8(b) an exactly equivalent plot is presented which is the more useful form for considering creep data. Here the creep rate (exactly equivalent to the strain rate) is plotted on the ordinate and stress level is plotted on the abscissa.

At low stress levels, the viscosity of the dashpot η_1 in Fig. 3(c) is much larger than that of the dashpot η_2. Hence η_1 can be regarded as infinite and model 3(c) reduces to model 3(a), the Eyring formulation of a standard linear solid[9]. The apparent critical stress can now also be explained in a more satisfactory fashion. Because of limitations imposed by the creep test itself, it is not practicable to measure strain rates below $\sim 10^{-9}s^{-1}$. There is hence a practical cut-off at very low strain rates, where the plateau creep rates are very small, and plateau creep behaviour would only be observed at very long times ($\sim$ several years). The apparent critical stress corresponding to these very low strain rates has been indicated schematically in Fig. 8(b). At these low stress levels we would also expect to find almost total recovery in terms of the modelling proposed here, and this expectation has been borne out by experiment[5].

RELATIONSHIP OF CREEP BEHAVIOUR TO STRUCTURE

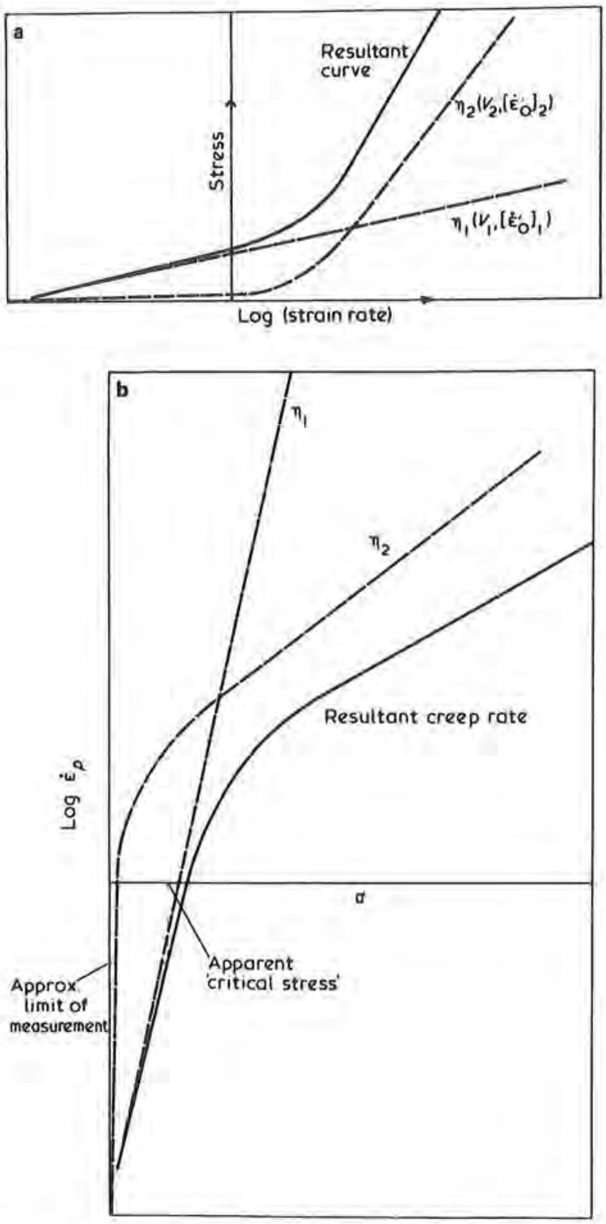

Fig. 8. Schematic representation of plastic flow for the 2-process model; (a) yield stress vs applied strain rate; (b) creep strain rate $\dot{\varepsilon}_p$ vs applied stress. (Reproduced from Polymer 22, 870 (1981) by permission of the publishers, Butterworth & Co. (Publishers) Ltd. (C)).

RELATIONSHIP OF CREEP BEHAVIOUR TO STRUCTURE

At high stress levels, equation (2) gives the relationship between the plateau creep rate and stress in terms of an apparent single activated process as

$$\frac{\sigma}{T} = \frac{k}{v_{eff}} \left\{ \frac{\Delta H_{eff}}{kT} + \ln \frac{2\dot{\varepsilon}_p}{[\dot{\varepsilon}_o]_{eff}} \right\} \quad (3)$$

where v_{eff} and ΔH_{eff} are the effective activation volume and activation energy respectively.

Because the term σv_{eff} is small, small variations in v_{eff} with temperature can be neglected and plateau creep rates determined at a constant stress level can be described by the equation

$$(\log \dot{\varepsilon}_p)_\sigma = \log [\dot{\varepsilon}_o]_{eff/2} - \frac{\Delta G_{eff}}{2.3kT} \quad (4)$$

where ΔG_{eff} is an activation free energy.

Results for two samples (Rigidex 50, λ=20 and Rigidex H020, λ=20) are shown in Fig. 9. There is a good linear relationship between log $\dot{\varepsilon}_p$ and 1/T, giving a value for ΔG_{eff} of 28 kcals/mole. Assuming a constant activation volume v_{eff} of 100Å^3 gives a value of 30 kcals/mole for ΔH_{eff}. This is in the range quoted for the α-relaxation in polyethylene by previous workers on the basis of dynamic mechanical experiments[10-12]. Now

$$\Delta H_{eff} = \frac{v_2 \Delta H_1}{v_1+v_2} + \frac{v_1 \Delta H_2}{v_1+v_2} \quad (5)$$

so that ΔH_{eff} is primarily determined by ΔH_2 (unless ΔH_1 is very much larger than ΔH_2). It is therefore reasonable to conclude that the smaller activation volume process relates to the α-relaxation process.

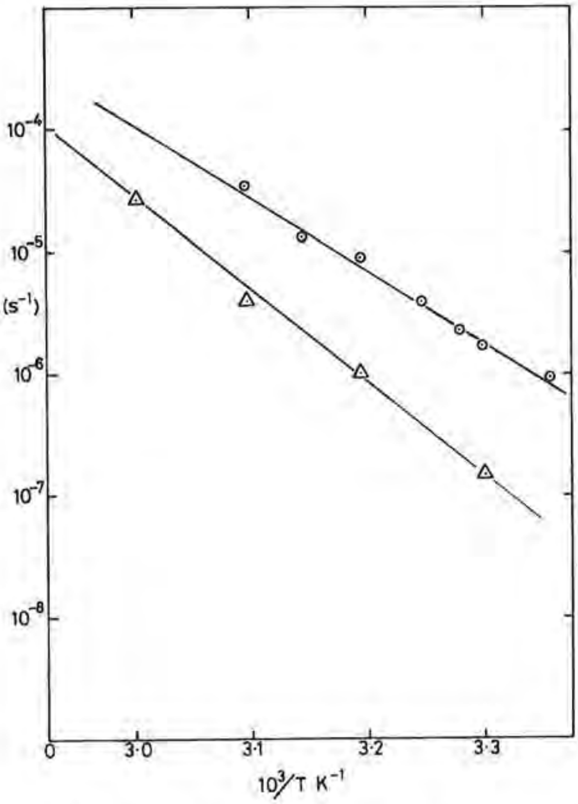

Fig.9. Temperature dependence of plateau creep rates $\dot{\varepsilon}_p$ for two samples Δ Rigidex 50, λ=20, stress level 0.1 GPa; Θ Rigidex H020, λ=20, stress level 0.25 GPa. (Reproduced from J.Polym.Sci., Polym. Phys. Edn., (in press).

To examine the changes in behaviour which occur on changing the structure of the oriented polymer, plateau creep data at 20°C for a number of different samples were fitted to the constant temperature form of equation (2)

$$\frac{\sigma}{T} = \frac{k}{v_1} \left\{ \ln \dot{\varepsilon}_p - \ln \left[\frac{\dot{\varepsilon}_o'}{2}\right]_1 \right\} + \frac{k}{v_2} \sinh^{-1} \frac{\dot{\varepsilon}_p}{[\dot{\varepsilon}_o']_2} \quad (6)$$

where $[\dot{\varepsilon}_o']_1$ and $[\dot{\varepsilon}_o']_2$ include the temperature dependence exp $\Delta H/kT$ term.

It was shown that the data could be equally well fitted to either a variable value for v_1 or a constant average value for v_1 and that the latter constant affected the values obtained v_2 to a very small extent only[13]. The results of these fitting procedures for a fixed value of v_1 are shown in Table 2, and some of data

TABLE 2

Activation parameters for the 2-process model

Sample	v_1 (Å^3)	$[\dot{\varepsilon}_o']_1$ (sec^{-1})	v_2 (Å^3)	$[\dot{\varepsilon}_o']_2$ (sec^{-1})
		v_1 fixed (Temperature 20°C)		
Rigidex 50, λ=20	456	2.2×10^{-8}	78	1.0×10^{-6}
006-60, λ=10	456	2.1×10^{-9}	720	2.6×10^{-11}
006-60, λ=20	456	1.7×10^{-14}	126	7.8×10^{-7}
006-60, λ=30	456	2.1×10^{-16}	78	6.6×10^{-7}
H020-54P, λ=10	456	5×10^{-14}	98	1.3×10^{-6}
H020-54P, λ=20	456	8.4×10^{-18}	95	1.6×10^{-7}
γ-irradiated Rigidex 50, λ=20	456	1.1×10^{-16}	103	1.2×10^{-6}
002-55, λ=20	456	1.6×10^{-18}	88	4.7×10^{-7}

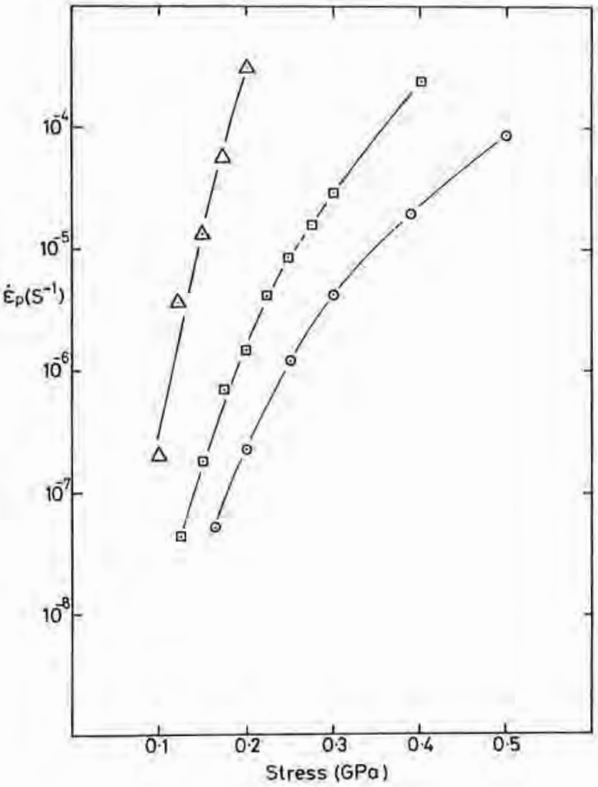

Fig. 10. Effect of draw ratio on plateau creep behaviour at 20°C for 006-60 samples
Δ λ=10, λ=20, ⊙ λ=30
(Reproduced from J.Polym. Sci., Polym. Phys. Edn., (in press).

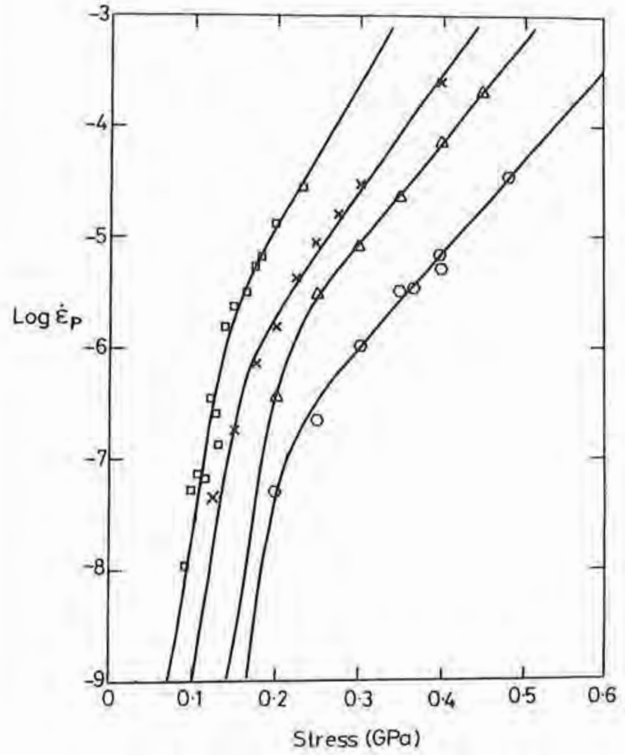

Fig. 11. Fitted curves to plateau creep data on the basis of the two process model, assuming that process 1 has an activation volume of 456Å³
Rigidex 50, λ=20, x 006-60, λ=20,
Δ γ-irradiated Rigidex 50, λ=20,
HO20, λ=20
(Reproduced from J. Polym. Sci., Polym. Phys. Edn., (in press).

(there is considerable overlap between results for several samples) in Figs. 10 and 11.

The differences between different materials are primarily reflected in the relative contribution of process 1, the large activation volume process. We note from Table 2 that the pre-exponential factor $[\varepsilon'_0]_1$ falls substantially with increasing draw ratio and there are large differences between samples of different chemical composition. In particular both γ-irradiated low molecular weight Rigidex 50 and the 002-55 copolymer behave like the high molecular weight HO20-55P. The activation volume of ∿ 500 Å³ for process 1 is consistent with that for an oriented non-crystalline polymer, and it has been suggested that this process is associated with the non-crystalline regions[5]. It is then attractive to speculate that γ-irradiation of low molecular weight polymer produces a comparable molecular network by incorporating chemical cross-links to that obtained in high molecular weight polymer due to physical entanglements. It is surprising that introducing a small proportion of branch points as in the 002-55 copolymer has the same effect. However, these results are consistent with observations of the tensile drawing of these materials. Increasing molecular weight, γ-irradiation prior to drawing and the introduction of side branches have all been shown to give rise to increased strain hardening[14-16].

With regard to the practical consequences of this work, it can be seen from Figs. 10 and 11 and Table 2 that although there is also merit in increasing the draw ratio, either increasing the molecular weight or γ-irradiation prior to drawing or introducing side branches, are equally effective in increasing the critical stress below which plateau creep cannot be observed within a sensible experimental time-scale. In the case of Tensar, a copolymer with a somewhat larger branch content than the Rigidex 002-55 grade was selected, to ensure a maximum critical stress compatible with achieving a good degree of molecular orientation by drawing.

CONCLUSIONS

The steady state creep behaviour of oriented polyethylene can be satisfactorily represented by two thermally activated processes acting in parallel. One process has a comparatively small activation volume and is primarily affected by the draw ratio, decreasing with increasing draw ratio. Its activation energy is close to that for the α-relaxation process, consistent with its identification with a deformation process in the crystalline regions of the polymer.

The second process has a comparatively high activation volume which is not significantly affected by changes in structure or chemical composition. The contribution of this process is markedly affected by the molecular weight of the polymer, by γ-irradiation prior to drawing and by branch content. It has been tentatively associated with the molecular network.

A result of practical importance is that for each drawn polymer, a critical stress can be defined, below which permanent flow is negligible and on unloading, recovery is virtually complete. This concept has been used to select a suitable polymer for Tensar and can also be applied to practical performance of Tensar grids, as described in a subsequent contribution to this symposium.

REFERENCES

1. Capaccio, G., Ward, I.M. (1973). Properties of ultra-high modulus linear polyethylenes. Nature Phys. Sci., 243, 130, 143; (1974) Preparation of ultra-high modulus linear polyethylenes; effect of molecular weight and molecular weight distribution on drawing behaviour and mechanical properties. Polymer, 15, 233.
2. Hannant, D.J. Symposium 'Polymers in Civil Engineering', Plastics & Rubber Institute, London 20th May, 1980.
3. Kamal, M. (1983). Ph.D. thesis Leeds University.
4. Ladizesky, N.H., Ward, I.M., Phillips, L.N. (1983). Novel fibre/resin interface for improved mechanical properties of composites reinforced with high modulus polyethylene filaments. Progress in Science & Engineering Composites, T. Hayashi, K. Kawata & S. Umekawa, Ed. ICCM-IV, Tokyo, 203-210.
5. Wilding, M.A., Ward, I.M. (1978). Tensile creep and recovery in ultra-high modulus linear polyethylenes. Polymer, 19, 969; (1981). Creep and recovery of ultra-high modulus polyethylene. Polymer, 22, 870. (1981). Routes to improved creep behaviour in drawn linear polyethylene. Plastics & Rubber Processing & Applications, 1, 167.
6. Sherby, O.D., Dorn, J.E. (1956). Anelastic creep of poly methyl-methacrylate. J. Mech. Phys. Solids, 6, 145.
7. Roetling, J.A. (1965). Yield stress behaviour of polymethylmethacrylate. Polymer, 6, 311.
8. Bauwens-Crowet, C., Bauwens, J.C., Homes, G. (1969). Tensile yield-stress behavior of glassy polymers. J. Polym. Sci., A2, 7, 735.
9. Halsey, G., White, H.J., Eyring, H. (1945). Mechanical properties of textiles, 1. Text. Res. J. 15, 295.
10. Sandiford, D.J.H., Wilbourn, A.H. (1960). "Polyethylene" (A. Renfrew & P. Morgan, eds) Iliffe, London, Ch.8.
11. Kajiyama, T., Okada, T., Sakoda, A., Takayanagi, M. (1973). Analysis of the α-relaxation process of bulk crystallized polyethylene based on that of single crystal mat. J. Macromol. Sci. Phys., B7, 583.
12. Nakayasu, H., Markowitz, H., Plazek, D.J. (1961). The frequency and temperature dependence of the dynamic mechanical properties of a high density polyethylene. Trans. Soc. Rheol. 5, 261.
13. Wilding, M.A., Ward, I.M. (1984). Creep behaviour of ultra high modulus polyethylene: Influence of draw ratio and polymer composition. J. Polym. Sci., Polym. Phys. Edn., (in press).
14. Capaccio, G., Crompton, T.A., Ward, I.M. (1976). The drawing behaviour of linear polyethylene. I. Rate of drawing as a function of polymer molecular weight and initial thermal treatment. J. Polym. Sci., Polym. Phys. Edn. 14, 1641. (1980). Drawing behaviour of linear polyethylene. II. Effect of draw temperature and molecular weight on draw ratio and modulus. J. Polym. Sci., Polym. Phys. Edn., 18, 301.
15. Capaccio, G., Ward, I.M., Wilding, M.A. (1978). The plastic deformation of γ-irradiated linear polyethylene. J. Polym. Sci., Polym. Phys. Edn., 16, 2083.
16. Capaccio, G., Ward, I.M. (1984). The drawing behaviour of polyethylene copolymers. J. Polym. Sci., Polym. Phys. Edn., (in press).

The load-strain-time behaviour of Tensar geogrids

A. McGown, K. Z. Andrawes and K. C. Yeo, *University of Strathclyde,* and D. DuBois, *Netlon Ltd*

TENSAR geogrids are a new generation of soil reinforcing materials manufactured by heat stretching a perforated sheet of co-polymer to form a grid-like structure. In order to use them to their maximum efficiency it is necessary to establish the loads which they may carry for any period up to 120 years, the design lifetime of many civil engineering structures. In this paper the basic definitions that should be used to describe the geometry of the grids are given and then employed to identify the representative sizes and shapes of test specimens. Test methods which have been developed for quality control purposes and for performance data acquisition are detailed. Following this the method of analysing and presenting test data are given together with typical data for both uniaxial and biaxial grids.

INTRODUCTION

Soils have little or no tensile resistance; therefore inclusion of tension-resistant materials within the soils is an effective means of reinforcing them. To optimise the efficiency of these inclusions, they should be placed in the zones of largest tensile strains and in the directions of principal tensile strains. The mechanism of stress transfer from the soil to the inclusion depends primarily on the geometrical properties of the inclusions. For rods, strips and sheets, the stress transfer mechanism is one of surface friction; but for grids, nets and meshes, it depends upon the more efficient interlock principle. When stressed, the inclusions must of course be capable of sustaining the load without rupture and without generating unacceptably large deformations during the design lifetime of the structure. Thus the two properties of tension resistant soil inclusions which must be established in order to allow the design of reinforced soil structures are their surface friction or interlock properties and their load-strain-time behaviour over the lifetime of the structure.

Tensar geogrids are molecularly oriented polymeric grid structures specifically developed for use as tension-resistant inclusions in soils. Jewell et al (1984) deal with the measurement of the interlock that develops between Tensar geogrids and various soil types. In this paper the methods of measuring and presenting the load-strain-time behaviour of the geogrids are detailed and their applicability to civil engineering specifications and designs is fully identified.

MATERIALS TESTED

In order to develop and prove the methods of testing and the analysis of test data for geogrids, control batches of two geogrids, Tensar SR2 and SS2, were used throughout. Tensar SR2 is a uniaxial geogrid manufactured from copolymer grade high density polyethylene (H.D.P.E.). Tensar SS2 is a biaxial geogrid manufactured from homo-polymer polypropylene. Prior to the production of both these grids, 2.5% of carbon black was added to provide ultraviolet protection.

The terminology used to describe the sizes and shapes of Tensar SR2 and SS2 is as shown in Fig. 1 and the mean dimensions of the materials in the control batches are given in Table 1, together with the mass per unit area of each product.

CLAMPING ARRANGEMENTS AND TEST SPECIMEN SIZES

In order to determine the load-strain-time relationship properties of the geogrids, specialised end clamps were developed, as shown in Fig. 2. The top and bottom bars of uniaxial grid test specimens are held directly by these clamps but the cross ribs of biaxial grid test specimens are cast into the clamps using a low melt point alloy "Ostalloy 158", manufactured by Fry's Metal Limited, Glasgow. The composition and properties of the alloy are given in Table 2.

By a programme of constant rate of strain testing at 2% strain per minute, 20°±2°C, and 65%±2% relative humidity, the minimum sizes of test specimens at which the measured load-strain properties of the grids are independent of sample size were established to be as shown in Table 3. These test specimen sizes are used in all subsequent testing.

CONSTANT RATE OF STRAIN TESTING

A constant rate of strain of 2% per minute and standard test conditions of 20°±2°C and 65%±2% relative humidity were used to establish reference load-strain properties for the geogrids. These properties are termed the "Index Properties". The effect of humidity on the properties of Tensar geogrids is negligible, but as with all polymeric materials, their load-strain properties vary with strain rates and temperature.

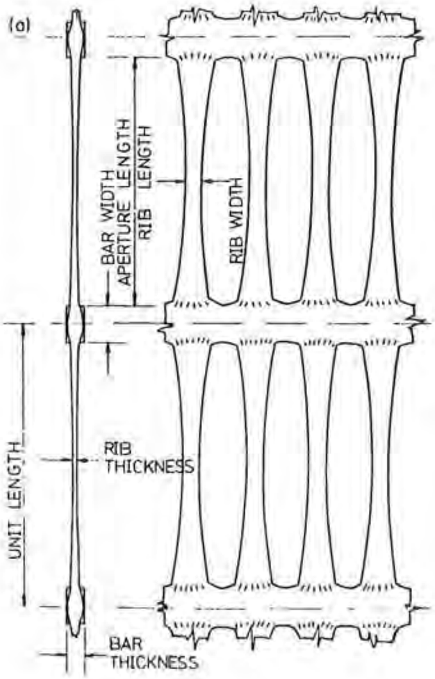

FIG. 1(a). TERMINOLOGY USED FOR TENSAR GEOGRID STRUCTURE, SR2.

TABLE 1. PHYSICAL PROPERTIES OF TENSAR SR2 AND TENSAR SS2

Dimensional Properties	Mean
Product Width	1000 mm
Number of Ribs	44 per metre
Aperture Length	90.73 mm
Transverse Bar Width	12.69 mm
Transverse Bar Thickness (max)	4.56 mm
(min)	4.36 mm
Rib Thickness	1.34 mm
Rib Width	5.72 mm
Product Mass	
Mass per unit area	971.6 g/m²

(a) TENSAR SR2

Dimensional Properties	Mean
Product Width	3000 mm
Number of Ribs (primary)	37 per metre
Number of Ribs (secondary)	27 per metre
Max. Aperture Length	34.42 mm
Max. Aperture Width	24.73 mm
Min. Rib Width (primary)	2.68 mm
Min. Rib Width (secondary)	2.95 mm
Grid Pitch (primary)	36.17 mm
Grid Pitch (secondary)	27.23 mm
Min. Rib Thickness (primary)	1.54 mm
Min. Rib Thickness (secondary)	1.74 mm
Max. Junction Thickness	4.17 mm
Product Mass	
Mass per unit area	202.6 g/m²

(b) TENSAR SS2

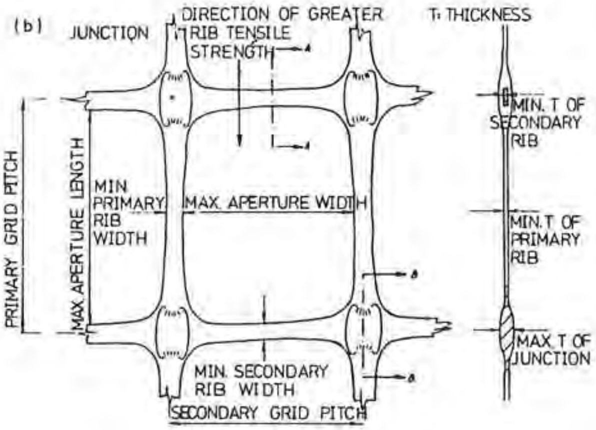

FIG. 1(b). TERMINOLOGY USED FOR TENSAR GEOGRID STRUCTURE, SS2.

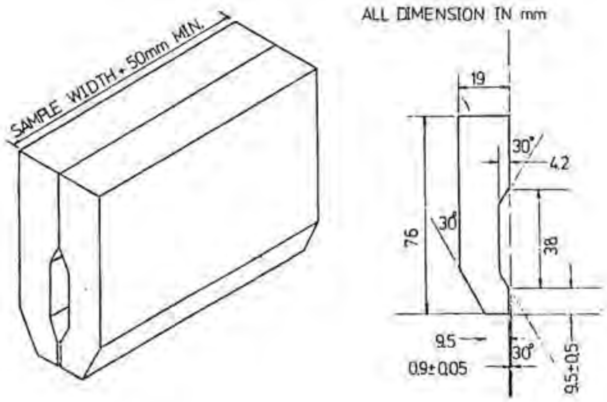

FIG. 2. ISOMETRIC VIEW AND HALF SECTION OF THE TENSAR JAWS.

The Index properties of Tensar SR2 and SS2 are as shown in Fig. 3. Corrections must be applied to these Index properties to obtain the constant rate of strain, load-strain properties at any other test conditions. The temperature and strain rate corrections for Tensar SR2 and SS2 are as given in Figs. 4 and 5 respectively.

TABLE 2. PHYSICAL PROPERTIES OF OSTALLOY 158

Melting temperature °C	70
Density g/cm	9.38
Specific heat liquid j/g°C	0.167
solid j/g°C	0.167
Latent heat of fusion KU/kg	32.564
Brinell hardness number	9.2
Tensile strength mpa	41.3
% elongation in slow loading	200
Loading mpa	
Max. load 30 secs.	68.9
Max. load 5 mins.	27.6
Safe sustained load	2.1
Composition %	
Bismuth	50.0
Lead	26.7
Tin	13.3
Cadmium	10.0

TABLE 3. TEST SPECIMEN SIZES FOR GEOGRIDS

Grid		Specimen Size
Uniaxial Product SR2		5 bars x 15 ribs
Biaxial Product		Vertical Ribs x Horizontal Ribs
SS2	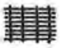	4 x 8 (secondary direction)
	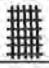	5 x 6 (primary direction)

Even with the slowest practical rates of strain of 10^{-3} to 10^{-4}% per minute in constant rate of strain testing, the time to reach strain levels operating in grids within soil structures is often no more than 1-2 months. Thus, there is a practical limit to the usefulness of constant rate of strain testing for the prediction of the long-term load-strain behaviour of geogrids. A more suitable means of determining this is creep testing.

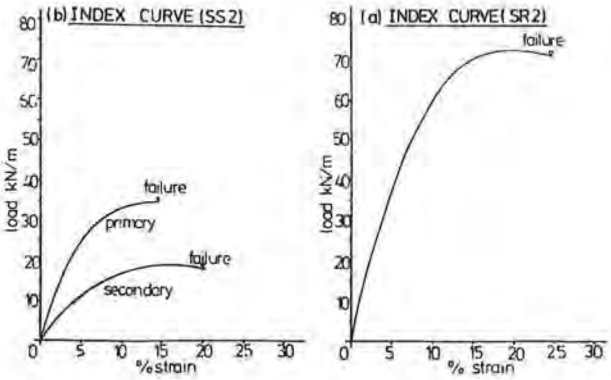

FIG. 3. INDEX TEST CURVES (a) SR2; (b) SS2.

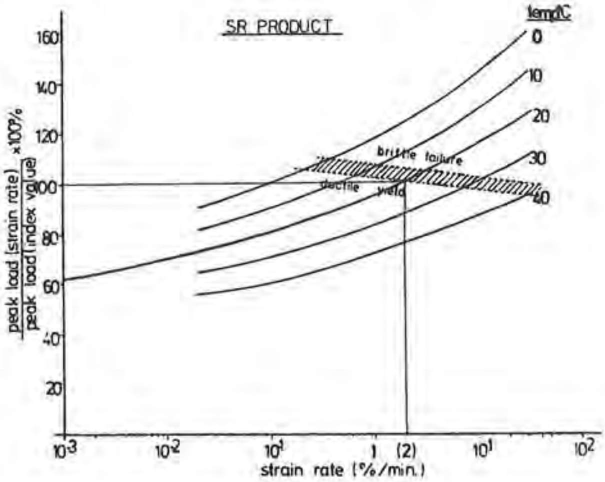

FIG. 4. TEMP/STRAIN RATE CORRECTION FOR SR2.

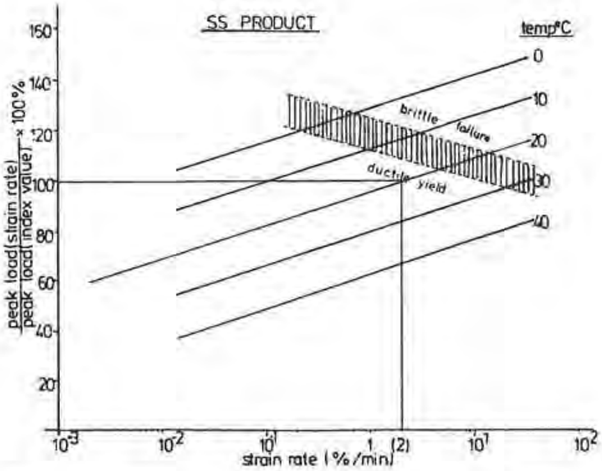

FIG. 5. TEMP/STRAIN RATE CORRECTION FOR SS2.

RAPID LOADING CREEP TESTING

(a) Test Method

To determine the long-term load-strain properties of Tensar geogrids, rapid loading creep tests were performed. Temperature and relative humidity conditions are controlled throughout the tests ±2°C and ±2% respectively. In each test the load is applied smoothly in less than 5 seconds, either by direct dead loading or through an adjustable 5 to 1 level arm system. The loads are maintained for the duration of the test at ±1% of full load, with continuous electronic monitoring undertaken. The deformation of the test specimen is measured electronically over the initial rapidly varying part of the test using two LVDT's, one each end of the specimen, but thereafter measurements are made by mechanical dial gauges at the same locations. To record the variations in load and deformations during the test, an electronic data logging device is used which records the output of the load cell and LVDT's in a pre-set pattern varying from every 0.2 seconds for the first 10 seconds to once per day after 24 hours.

The data obtained from each test is plotted as load against time and strain against time, with at least five levels of load applied at each test temperature. The range of test temperatures presently used is from 0°C to +40°C. The duration of loading is usually in excess of 1000 hours, unless rupture of the test specimen occurs before the allotted period of testing. Where rupture does not occur, tests are terminated when the daily creep strain rate either reaches a minimum value or becomes insignificant (i.e. when the $\log_{10}$ value of the strain rate is less than the order of -8 . The unit of strain rate is % strain/min.). At the end of each test period, the test specimen is partially unloaded and left under reduced sustained loading for 100 hours, to establish the elastic rebound of the material. During the unloading and reduced loading period, the load and deformation of the test specimen is measured in the same manner as during loading. Normally a number of short term load tests of five hours duration with partial unloading sustained for a half hour are also conducted to improve the interpretation of the initial loading and unloading behaviour of these materials.

(b) Presentation of Test Data

The load-strain-time behaviour of geogrids at any temperature (T°C) can be represented by a rheological model which is as shown in Fig. 6. This comprises both recoverable (elastic) and irrecoverable (plastic) instantaneous strains and linear and non-linear time-dependent creep strains. In order to assess these various components of the total strain it is, however, necessary to perform a correction to the initial part of the rapid loading creep test data to establish an equivalent instantaneous loading strain-time curve, as shown in Fig. 7(a). In the same manner, the rapidly unloaded test data is corrected to establish an equivalent instantaneous unloading strain-time curve, as shown in Fig. 7(b). Having corrected the strain-time test data in this manner, equivalent instant-

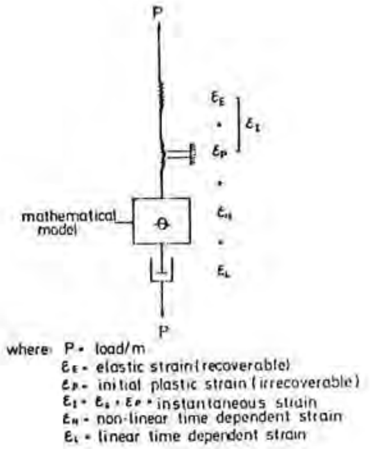

FIG. 6. RHEOLOGICAL MODEL.

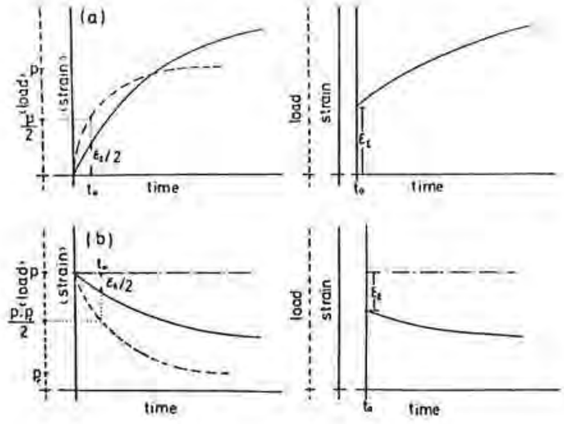

FIG. 7. INSTANTANEOUS CREEP DATA CORRECTION FOR (a) LOADING and (b) UNLOADING.

aneous strain-time curves may be produced, as is shown in Fig. 8 for Tensar SR2. Similar unloading curves may also be produced after appropriate corrections to the unloading test data.

A further method of presenting the test data at any temperature is to plot the daily creep strain rate on a logarithmic scale against the cumulative strain, as shown in Fig. 9 for Tensar SR2, Wilding and Ward (1978). This plot clearly indicates whether the daily strain rate is reaching a minimum value or approaching zero and so determines the duration of the test. It also provides data for identifying the linear creep strain component of the rheological model and other important performance limits which will be discussed in the following sections.

From the basic strain-time plots, the short and long-term creep test data at any temperature, the instantaneous loading and unloading strain parameters for the range of applied loads are obtained as shown in Fig. 10. From the log strain rate versus strain plot, the minimum daily creep strain rate is established for the various applied loads and used to calculate the linear creep strain component of the rheological model. Knowing the instantaneous and linear creep strain components of the total strain, the non-linear creep strain at any time and load may be obtained by difference, and then characterised using curve fitting techniques. Thus the overall strains for any load at any time and temperature can be modelled. By repeating this process for the test data at various temperatures then temperature corrections to the various parameters within the rheological model are obtained.

LOAD-STRAIN-TIME RELATIONSHIPS

Both the constant rate of strain test data and the creep test data, supplemented by data generated from rheological modelling, may be used to identify the load required to produce any strain after a period of time at any operating temperature. Due to the limitations of the period of testing in constant rate of strain tests, creep testing has been chosen as the preferred method of obtaining these data.

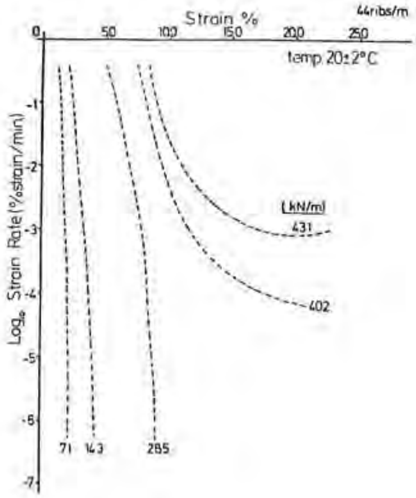

FIG. 9. LOG_{10} STRAIN RATE vs. STRAIN PLOTS FOR SR2.

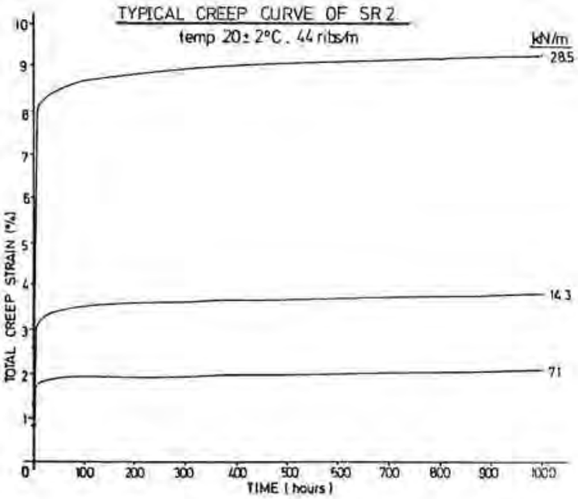

FIG. 8. TYPICAL STRAIN-TIME CURVES FOR INSTANTANEOUS LOADING FOR SR2.

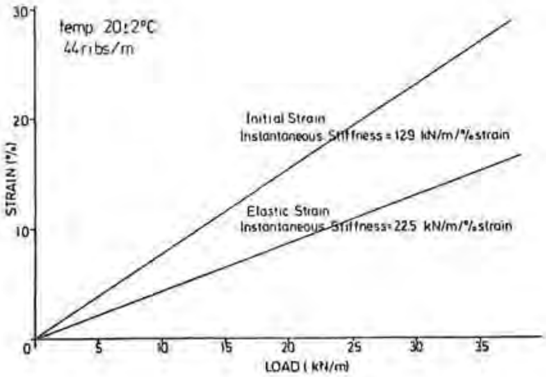

FIG. 10. RHEOLOGICAL MODEL COMPONENTS FOR SR2 (INITIAL STRAIN ε_I and ELASTIC STRAIN ε_E.

The data are best plotted as isochronous-strain curves for each test temperature in the manner indicated in Fig. 11 for Tensar SR2 and SS2 at 20°C. As can be seen from Fig. 11(a), the isochronous load-strain relationship for Tensar SR2 is approximately linear up to 10% strain. The log strain rate versus strain plot of creep test data for Tensar SR2 at the same temperature, Fig. 9, also shows that below 10% strain, this geogrid shows no tendency to approach creep rupture for the range of applied loads. Thus for Tensar SR2 at 20°C, 10% strain represents its "Performance Limit Strain" below which rupture is not likely to occur by ductile yield. Also up to 10% strain, the isochronous stiffness of the geogrid (i.e. the ratio of load to strain at given times) may be represented by the secant slopes of the isochronous load-strain curves. These may be replotted as isochronous stiffness against time, as shown in Fig. 12 for Tensar SR2 at 20°C.

The maximum load that may be sustained for any given time by a geogrid without approaching creep rupture is simply calculated by multiplying the performance limit strain by the isochronous stiffness at the given time. In the case of the Tensar SR2 control batch, this gives for 120 year lifetime a maximum load of 29 kN/m. For any given period of time significantly less than this, the maximum load that may be carried is greater than this value.

Alternatively by assuming that creep under constant load occurs in the geogrid when it is in the soil, then for loads less than the maximum value, the strain developed at any given time is calculated by dividing the load by the isochronous stiffness at that time. Thus the isochronous stiffness data may be used to reconstruct the creep strain-time data for any load. Alternatively, should the geogrid be assumed to suffer load relaxation when in-soil (i.e. reduction in sustained load at constant strain) the rheological model may be used to generate mathematically the reduction in load in the geogrid with time. For Tensar SR2 this is shown in a normalised form in Fig. 13.

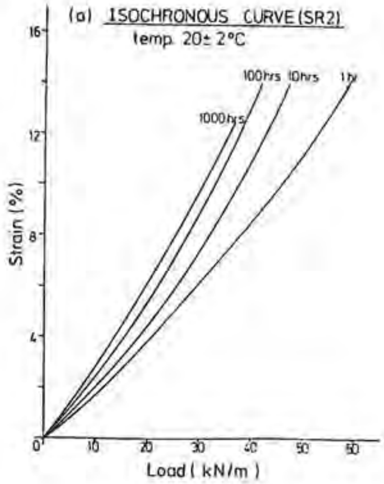

FIG. 11(a). ISOCHRONOUS LOAD-STRAIN CURVES FOR SR2.

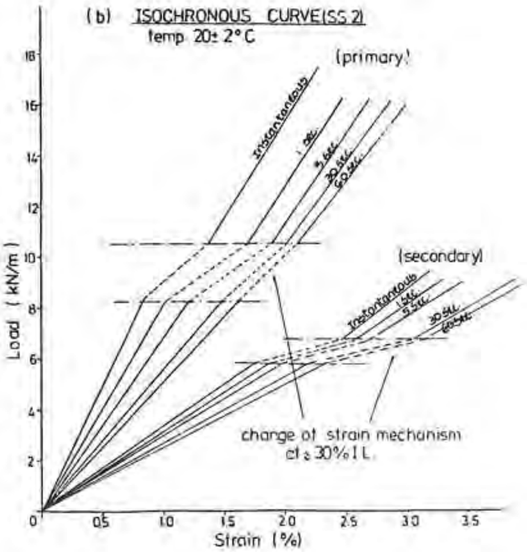

FIG. 11(b). ISOCHRONOUS LOAD-STRAIN CURVES FOR SS2 (BOTH DIRECTIONS).

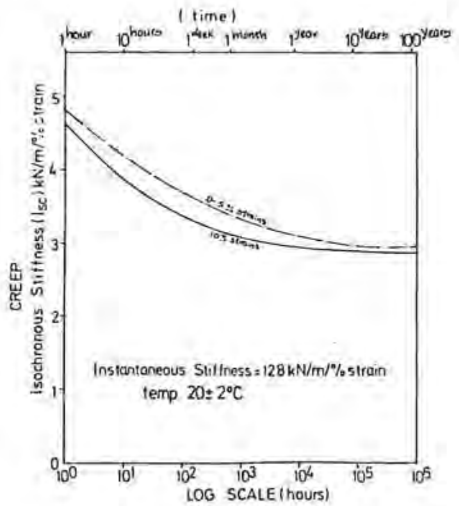

FIG. 12. ISOCHRONOUS STIFFNESS vs. TIME FOR SR2.

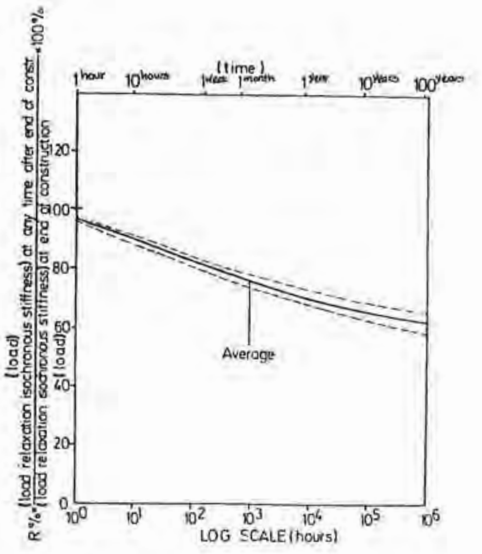

Generated Mathematically (temp. 20°C)

FIG. 13. LOAD RELAXATION NORMALISED vs. TIME FOR SR2

USE OF DATA IN SPECIFICATIONS AND DESIGNS

The constant rate of strain test data carried out under standardised Index conditions, provide a very useful set of data on which the civil engineer may base his specification of product quality. This may be based on the entire load-strain index curve, on peak values or on specific loads to be attained for particular strains. In each case, the characteristic value rather than the mean value is best specified (i.e. the value which has a 95% confidence of being achieved; CIRIA Report No. 63 (1977).

These Index data may also be used in designs which are purely empirical or based on back analysis, but where a more fundamental analytical approach is taken, the load-strain-time relationships developed from rapid loading creep testing must be used. By multiplying the isochronous stiffness with the likely strains to be developed in the soil system, up to the performance limit strain, the load that may be safely carried by a geogrid for any period of time may be calculated and employed in the analysis of any soil-geogrid structure. Additionally the construction and post-construction deformations may be calculated using these data by assuming pure creep in the geogrid. Also from mathematically generated data the possible post-construction load-relaxation of the geogrid may be calculated. Thus the upper and lower bound conditions of post-construction behaviour of the geogrid can be calculated. The method of employing these data in designs is discussed in detail by McGown et al (1984).

CONCLUSIONS

The development work described in this paper confirms that in common with all polymeric materials, the load-strain behaviour of Tensar geogrids when tested under constant rate of strain, are significantly influenced by the test temperature and strain rate. The necessity of employing standardised test conditions is thus emphasised and convenient standardised Index Test Conditions have been identified. It is suggested that these provide data which may form a suitable basis for civil engineering specifications. Rapid loading creep tests have been shown to be suitable for the measurement of the load-strain-time relationship of the geogrids. Methods of presenting data from these tests in a form suitable for use in the design of soil-geogrid structures have also been developed. These allow the loads and strains in the geogrids at any time to be easily calculated.

The rapid loading creep test data allow the identification of the performance limit strains for the geogrids. Below these strains there is no risk of rupture by ductile yield in the geogrids at any time during the lifetime of the soil-geogrid structure. It must be noted, however, that a separate analysis must be undertaken to ensure that brittle fracture of the polymer does not occur. This analysis involves calculating the stresses within the polymer and ensuring that these are maintained at all times at levels below the critical brittle fracture stress.

ACKNOWLEDGEMENTS

The authors wish to acknowledge that this work was undertaken with the support of a Science and Engineering Research Council Co-operative Grant made in conjunction with Messrs. Netlon Limited.

REFERENCES

CIRIA Report 63. ((1977). Rationalisation of safety and serviceability factors in structural codes. Jul., 55-56.

Jewell, R., Milligan, G.W.E., Sarsby, R.W. and DuBois, D.D. (1984). The interaction between soil and geogrids. Proc. Symp. on Polymer Grid Reinforcement in Civil Engineering, Mar.

Paine, N., McGown, A., Jewell, R. and DuBois, D. (1984). The use of geogrid properties in design. Proc. Symp. on Polymer Grid Reinforcement in Civil Engineering, Mar.

Wilding, M.A. and Ward, I.M. (1978). Tensile creep and recovery in ultra-high modulus linear polyethylenes. Polymer, 19, 969-976.

Interaction between soil and geogrids

R. A. Jewell, *Binnie and Partners*, G. W. E. Milligan, *University of Oxford*, R. W. Sarsby, *Bolton Institute of Higher Education*, and D. Dubois, *Netlon Ltd*

Three mechanisms of interaction between soil and grid reinforcement have been identified to provide a framework for understanding and interpreting laboratory and field measurements. Their importance in governing the resistance to direct sliding of soil over grid reinforcement and the bond strength for different types of grid reinforcement has been examined. A qualitative model is proposed to classify the influence of soil particle size on soil grid interaction. Theoretical expressions have been developed to describe direct sliding resistance, bearing stresses, and bond strength of reinforcement in terms of well accepted soil and reinforcement parameters. The results have been compared with available laboratory and field data. Guidance is given on measuring values of grid sliding resistance and bond strength in the laboratory, and on the selection of parameters for design.

INTRODUCTION

Limit equilibrium analysis of reinforced soil focuses attention on the mechanisms or modes of behaviour which could lead to unsatisfactory performance. For example, in a reinforced slope gross outward sliding of soil over the surface of a reinforcement layer, or insufficient bond between the reinforcement and soil could lead to failure, Fig. 1. An analysis for these cases requires an understanding of the mechanism of interaction between soil and reinforcement, so that relevant parameters and their numerical values can be defined.

The case of grids reinforcing soil to provide stability in structures governed by self weight loading, such as the embankment in Fig. 1, is examined in the paper. The action of soil bearing on surfaces of the grid members plays a significant role in the interaction, but it is complex and as yet not well understood, Schlosser et al (1983).

The suitability of a grid form for soil reinforcement has been demonstrated by laboratory and field studies , Chang et al. (1977), Forsyth (1978), Peterson (1980). Over the past few years the availability of strong polymer grids with high extensional stiffness and resistance to corrosion has increased interest in grid reinforcement for soil. Their potential use in cohesive, low quality or aggressive soils is particularly attractive and has provided an incentive for research.

The results of the research have been examined to investigate the mechanics of soil grid interaction. A number of simple mechanisms have been identified which organise the experimental findings allowing simple parameters to be defined in terms of the grid geometry and conventional soil properties. These parameters can be evaluated by straightforward tests.

While it is clearly recognised that the mechanisms proposed in this paper radically simplify the complexities of real behaviour, the aim has been to provide a framework for the understanding of soil grid interaction so that it may be evaluated for design purposes.

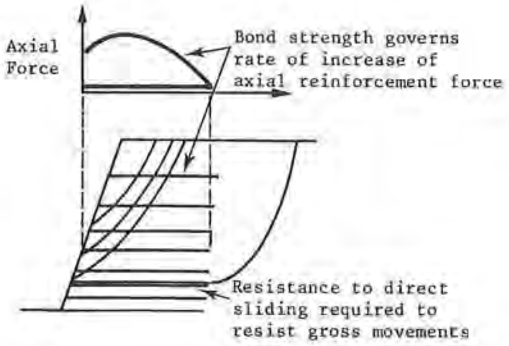

Fig.1. Two mechanisms of failure in a reinforced embankment.

GRID TYPES AND PARAMETERS

Three types of grid are shown in Fig. 2. A simple grid which has been tested in research investigations is formed by punching apertures into a plane sheet, Fig 2a. The grids formed from welded bars, Fig. 2b, and from drawn polymers, Fig. 2c, have been more widely used for research investigations and field constructions.

The parameters suggested to describe the geometry of a grid are illustrated in Fig. 3 for an element of grid length L_r and width W_r.

Polymer grid reinforcement. Thomas Telford Limited, London, 1985

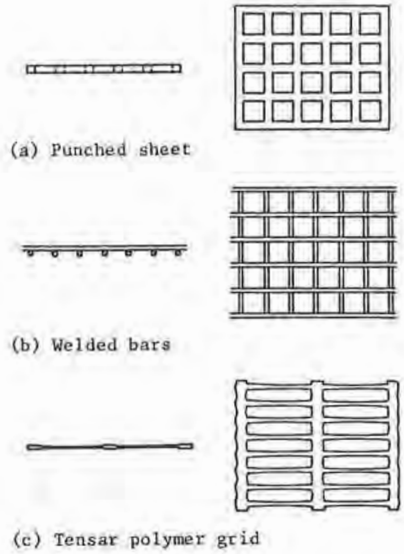

Fig.2. Three types of reinforcement grid.

The spacing between the members on which soil bearing may occur is denoted by S and the thickness of these bearing members by B. In plan, the total grid area is A_r and this comprises a fraction of solid material α_s and a fraction of apertures $(1 - \alpha_s)$. Depending on the type of grid, the full width of the members may be available for bearing, $\alpha_b = 1$ in the case of a welded grid, or only a fraction of the width $\alpha_b < 1$, as in the case of a punched sheet or a Tensar grid.

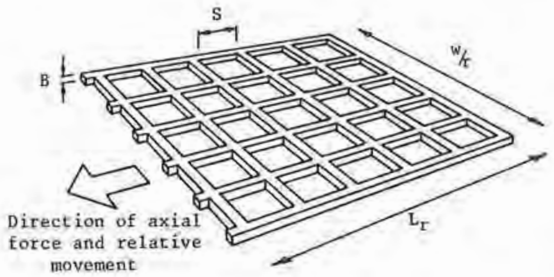

$A_r = W_r L_r$ Grid surface area

α_s Fraction of grid surface area that is solid

α_b Fraction of grid width W_r available for bearing

Fig.3. Definition of terms for a grid.

MECHANISMS OF INTERACTION

Two main modes of behaviour which need to be considered for design of a reinforced embankment are illustrated in Fig.1. Reinforcement layers must have sufficient length to prevent gross outward movement of soil blocks sliding across the surface of a reinforcement layer in the soil. Sufficient reinforcement length must also be provided to ensure that the required axial force may be developed in the reinforcements through bond to maintain satisfactory equilibrium. These two cases, direct sliding and bond strength, are examined in separate sections below.

Three main mechanisms of soil reinforcement interaction can be identified. These are,

- soil shearing on plane surfaces of the reinforcement which are parallel to the direction of relative movement of the soil
- soil bearing on (bearing) surfaces of the reinforcement which are substantially normal to the direction of relative movement of the soil
- soil shearing over soil through the apertures in a reinforcement grid.

For clarity, the action of these three mechanisms and their relative importance for direct sliding resistance and bond strength are examined separatly below.

DIRECT SLIDING RESISTANCE

The loading condition for direct sliding is a gross outward shearing force tending to cause a block of soil overlying a horizon of reinforcement to shear over the reinforcement and the underlying soil. The three mechanisms of interaction may each resist direct sliding as shown in Fig. 4.

Shear between soil and plane surfaces

The resistance provided by shear between soil and the plane surface areas of a grid, Fig. 4a, is similar to the skin friction that is measured conventionally for soils and construction materials. The most comprehensive series of measurements for skin friction were carried out by Potyondy (1961). He used a direct shear test with a block of the construction material mounted flush in the lower portion of the box and the soil in the upper half. The resistance to sliding is defined by an angle of skin friction δ. The test is now widely adopted as a standard method for measuring friction between soil and plane reinforcement surfaces, Schlosser & Juran (1979).

The ratio of skin friction to soil friction for sands and silts acting on smooth metallic or concrete surfaces is typically in the range $\delta/\phi = 0.5$ to 0.8, Potyondy (1961).

Soil bearing on reinforcement

The effect on overall direct sliding resistance of soil bearing on reinforcement surfaces is more difficult to assess, Fig. 4b.

To generate bearing stresses there must be relative movement between the soil and the reinforcement bearing surface. This implies that soil within the grid apertures would have to displace relative to the grid, Fig. 4b. From symmetry, the soil in the upper and lower halves of the grid apertures would need to move in opposite directions, shearing with respect to one another, so that bearing stresses could be balanced across a grid bearing member.

By choosing to concentrate shear displacement across the top of the grid, the soil contained in the grid apertures would not displace relative to the bearing members and resistance from bearing stresses could be avoided. This is illustrated in terms of rupture surfaces in Fig. 5. This suggests that soil bearing is unlikely to have a significant effect on direct sliding resistance for a grid in granular soils.

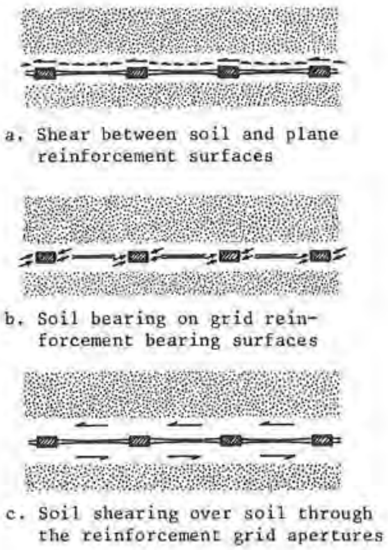

Fig.4. Three mechanisms resisting direct sliding.

Soil shearing over soil

In order for outward direct sliding to occur the overlying soil must shear with respect to the underlying soil and the grid. The resistance to shear in the aperture spaces of the grid should equal the resistance to direct shear of unreinforced soil ϕ_{ds}, which can be measured in a direct shear test.

Influence of soil particle size

The relative size of the soil particles to the grid apertures can influence direct sliding resistance in four main ways, and these are shown schematically in Fig. 5 for the case of a Tensar grid.

Soil made up of small particles in the fine sand or silt sizes has greater kinematic freedom to rupture in zones of varying orientations, so that an overall displacement can be made up from several components, Arthur et al (1977). In a fine soil the size of the rupture zone, which is about 25 particle diameters, and the shear displacement required to take the soil beyond peak resistance are both reduced, Roscoe (1970). These points are illustrated by the careful measurements in the simple shear apparatus of Bhudu (1979) .

Fine soil may thus take maximum advantage of the relatively smooth surface areas of a metal or polymer grid. In the case of a Tensar grid this would involve sliding across the surface of the thinner, load carrying rib members as well as across the top surface of the bearing members, Fig. 5a.

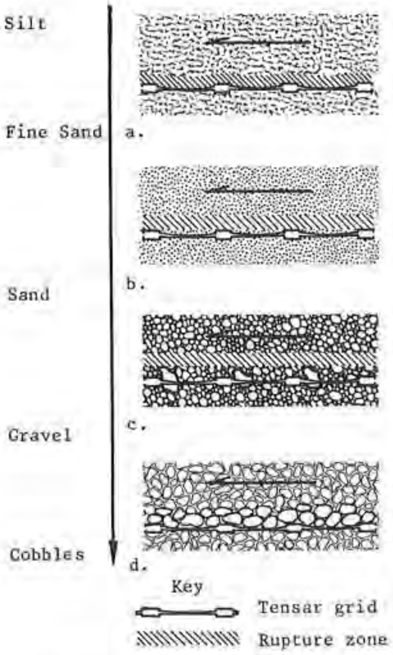

Fig.5. Qualitative effect of increasing soil particle size on direct sliding. View in cross-section across direction of sliding.

For a coarser sand, the potential advantage in terms of reduced direct sliding resistance of sliding on the smooth rib surface areas may be insufficient to compensate for the extra resistance of a rupture zone at varying orientations. The direct sliding mechanism would, in this case, change to a rupture zone formed mostly in the soil taking advantage only of the smooth top surface of the bearing members, Fig. 5b.

If the soil contains particles of a similar size to the grid apertures, then these may become lodged against the grid bearing members and extend into the soil on either side of the grid, Fig. 5c. If a number of particles were lodged in this way the soil would no longer be able to take advantage of the smooth top surface of the bearing members, and the rupture zone would be forced away from the grid fully into the soil. In this case the shear resistance to direct sliding would equal the full shear resistance of the soil.

Finally, grid reinforcement could be placed in soils with particles too large to penetrate the grid apertures, Fig. 5d. The resistance to direct sliding in this case could be very low indeed. In the extreme, shear resistance might be provided only by soil particles in contact with the plane grid surface areas. The irregularity in the surface profile of the grid in this case would be insignificant to the scale of the soil, so that little benefit from that source could be expected. The shear resistance to direct sliding could therefore be reduced to the resistance of the soil bearing on a smooth sheet of the parent reinforcement material, usually a metal or a polymer.

The influence of soil particle size on direct sliding resistance is shown qualitively in Fig. 6. Direct sliding resistance is expressed as a factored reduction on the soil direct shear resistance, $f_{ds}\tan\phi_{ds}$, as explained below.

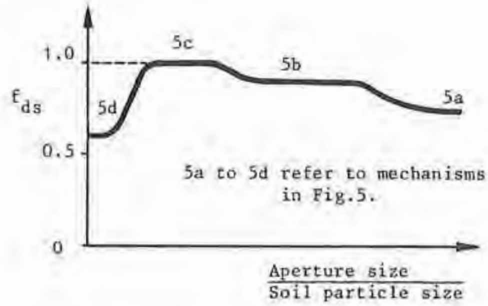

Fig.6. Schematic illustrations of the influence of particle size on the resistance to direct sliding, $f_{ds} \tan\phi_{ds}$.

<u>Theoretical expressions for direct sliding resistance</u>

The basic equation for direct sliding resistance can be expressed in terms of the two contributions from shear between soil and the plane surface areas of the grid, and between the soil shearing over itself in the grid apertures. Direct sliding resistance can be described by a general expression,

$$f_{ds}\tan\phi_{ds} = \alpha_{ds}\tan\delta + (1-\alpha_{ds})\tan\phi_{ds} \qquad (1)$$

where f_{ds} coefficient of resistance to direct sliding
ϕ_{ds} angle of friction for soil in direct shear
δ angle of skin friction for soil on plane reinforcement surfaces
α_{ds} fraction of grid surface area that resists direct shear with soil

The parameter α_{ds} has been introduced so that one general expression can be used to describe the four different values of direct sliding resistance envisaged,Fig.6. Equation (1) can be manipulated to give an expression for f_{ds},

$$f_{ds} = 1 - \alpha_{ds}\left(1 - \frac{\tan\delta}{\tan\phi}\right) \qquad (2)$$

The effect of the soil particle size shown in Figs. 5 & 6 can now be seen from equation (2). A reduction in the value α_{ds} results in an increase in direct sliding resistance f_{ds}, during the change from case 5a through 5b to 5c, Fig. 5. Indeed when the rupture zone is forced away from the grid, case 5c, $\alpha_{ds} = 0$ and $f_{ds} = 1.00$. In the extreme case of large particles resting directly on the grid plane surfaces rather than penetrating the apertures, case 5d in Fig. 5, $\alpha_{ds} = 1.00$ resulting in a reduction of direct sliding resistance to

$$f_{ds} = \frac{\tan\delta}{\tan\phi_{ds}}$$

For design of cases with reinforcement grids providing stability in embankments or retaining walls where the soil fill particles penetrate the grid apertures, a suitable value of maximum direct sliding resistance would be given by equations 1 or 2 adopting a value $\alpha_{ds} = \alpha_s$, where α_s is the fraction of solid surface area in a grid, Fig. 3. This corresponds to case 5a in Figs. 5 and 6.

<u>Comparison with experimental results</u>

A comprehensive series of tests have been carried out investigating the influence of particle size on direct sliding resistance. Two types of polymer grid Tensar SR1 and Tensar SR2 were used, Netlon Limited (1984). Seven different grading curves gave relative soil particle sizes ranging from silts to gravels.

The soil types are indicated on Fig. 7. Five of the soils were crushed limestone. Pulverised fuel ash provided a fine grained soil and crushed granite a uniformly coarse soil with an average particle size 8 mm.

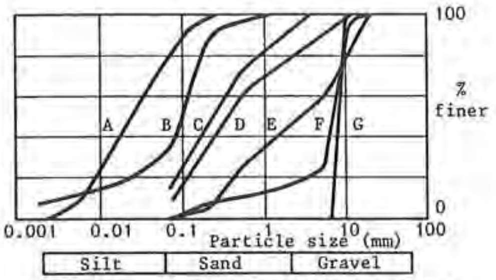

SOIL TYPE : A pulverised fuel ash

B to F crushed limestone G crushed granite

Fig.7. Soils tested during investigations of direct sliding resistance.

Direct shear tests were carried out in a large shear box. The lower portion of the box was first filled with compacted soil almost to the top, the grid placed so as to be flush with mid-plane of the shear box, then the upper half of the box was filled and a vertical load applied before shearing.

The results of tests on the grid Tensar SR2 with an aperture width 17.3 mm are summarised in Fig. 8. The coefficient of direct sliding resistance f_{ds} for peak conditions (the ratio of peak resistance for sliding over the grid and soil to the peak direct shear resistance of the soil alone) is shown plotted against the ratio of aperture width to the average or D_{50} particle size.

At low ratios of aperture width to soil particle size, tests were carried out on soil type G and the grid Tensar SR1. The test results were obtained with one grid type by clipping out alternate rib members and then pairs of rib members, and the results are summarised in Fig. 9.

The trend of the results shown dotted in Figs. 8 and 9 confirm the expected variation of direct sliding resistance with soil particle size.

Predictions using equation (2) for the direct sliding resistance of Tensar SR2 in crushed limestone can be compared with the experimental measurements. The ratio of peak skin friction angle to peak soil friction angle for crushed limestone (grading C in Fig. 7) on a high density polyproplene sheet was measured to be

$$\frac{\tan\delta}{\tan\phi_{ds}} = 0.63$$

The ratio of the area of solid grid surfaces to the total area of the grid for Tensar SR2 is $\alpha_s = 0.46$, Netlon Limited (1984). For the case of soil shearing over the top surface of bearing members the ratio of area reduces to $\alpha_{ds} = 0.12$.

Using equation (2), the predicted resistance to direct sliding in fine soil is,

$$f_{ds} = 1 - 0.46\ (1 - 0.63) = 0.83 \qquad (3)$$

In coarser soil,

$$f_{ds} = 1 - 0.12\ (1 - 0.63) = 0.96 \qquad (4)$$

When soil particles larger than the bearing member thickness can penetrate the grid apertures and lodge against the bearing member, the rupture zone is forced away from the grid so that,

$$f_{ds} = 1 - 0.00\ (1 - 0.63) = 1.00 \qquad (5)$$

Finally for large soil particles resting on the grid surfaces and not penetrating the apertures,

$$f_{ds} = 1 - 1.00\ (1 - 0.63) = 0.63 \qquad (6)$$

The values given by equation (2) are shown on Figs. 8 and 9 to bound the experimental data well.

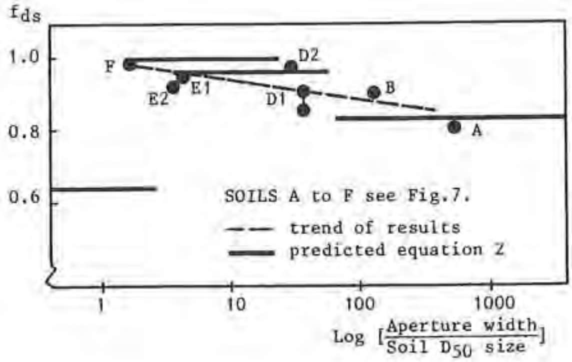

Fig.8. Measured peak direct sliding resistance f_{ds} for granular soils over Tensar SR2 grid reinforcement.

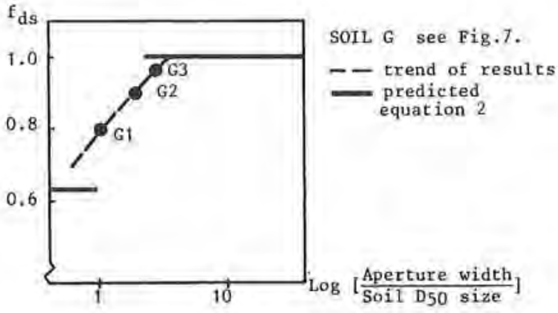

Fig.9. Measured peak direct sliding resistance f_{ds} for granular soil over Tensar SR1 grid reinforcement.

On the basis of the data available, it is recommended that equation (2) with a value $\alpha_{ds} = \alpha_s$ would give a suitably conservative value of direct sliding resistance for design when,

$$\frac{\text{Minimum Aperture Dimension}}{\text{Average Soil Particle Size}} \geq 3 \qquad (7)$$

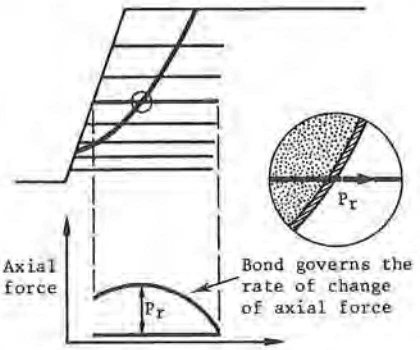

Fig.10. Bond strength governs the reinforcement length to mobilise axial reinforcement force.

BOND STRENGTH

The rate of change of axial force in reinforcement embedded in soil is limited by bond strength. For reinforcement in an embankment or retaining wall the changes in axial force close to the free end of the reinforcement embedded in the soil are important for determining the necessary lengths to enable the required axial forces to be generated. This is illustrated in Fig. 10.

Axial reinforcement force is caused by the development of linear soil strains in the direction of the reinforcement. A stiff reinforcement will resist such strains which, in the case of tensile strain in reinforced soil, results in axial tensile force in the reinforcement.

Since there is no relative displacement of soil on either side of the reinforcement, only two of the three simple mechanisms of interaction apply, namely

- soil shearing on plane surface areas of the reinforcement, and
- soil bearing on reinforcement surfaces (bearing surfaces) substantially normal to the direction of relative movement between the soil and the reinforcement.

These two mechanisms are illustrated in Fig. 11 for the case of bond, and are considered separately below.

Shear between soil and plane surfaces

The comments that were made for the case of direct sliding resistance should apply equally here. The shear stress that can be developed would depend on the angle of skin friction and the normal effective stress between the soil and the reinforcement surface.

When a rough bar or strip is pulled out from dense granular soil, volume expansion accompanies shear in the rupture zone that develops in the soil next to the reinforcement surface.This volume change can locally increase the normal effective stress and the resistance provided by shear between soil and the reinforcement surface. The phenomenon has similarities to the changes in stress that occur during a cavity expansion test in soil.

Whether the local increase in normal effective stress observed in pullout tests occurs when reinforcement acts under self-weight soil loading (rather than pullout loading), and whether, if it does, the increase in stress should be relied upon for design calculations has been and continues to be debated, Schlosser & Juran (1979), Schlosser et al (1983).

For grid reinforcement it may be prudent from the outset to estimate the normal effective stresses acting on the grid surface from self-weight and external loadings only.

The shear stress component of bond for a reinforcement grid of length L_r of width w_r placed horizontally in soil under self-weight loading would provide a maximum force,

$$(P_r)_{\text{shearing}} = 2\, A_r \alpha_s \,.\gamma z.\tan\delta \qquad (8)$$

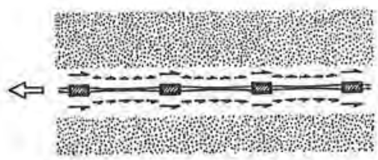

a. Shear between soil and plane surfaces

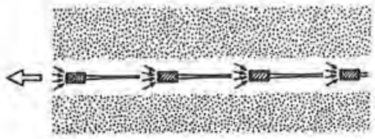

b. Soil bearing on reinforcement surfaces

Fig.11. The two mechanisms for bond between a grid and soil.

Soil bearing on grid surfaces

The bearing stress of soil on grid members is a problem similar in kind to the base pressure on deep foundations in soil. Kerisel (1961) concluded from test data that the soil density, foundation depth and size of bearing area have an important influence on bearing pressures, and that these are not a function only of soil friction angle. Vesic (1963) reported test results for which the ultimate bearing pressure for deeply embedded footings appeared to depend only on the relative density of the sand. Vesic observed a punching failure mode for footings in medium dense and loose sand models which resulted in significantly lower bearing pressures.

The bearing stresses on vertical surfaces loaded horizontally have been studied for the case of anchor plates. Rowe & Davis (1982) reported extensive numerical investigations based on the finite element method giving results which compared well with available data from anchor tests.

Selection of boundary conditions

The bearing members of a grid, can be thought to be like a line of anchors at a spacing S, Fig. 12a. The grid thickness B is likely to be small in comparison to the depth of soil z, and for most cases the bearing members can be considered deeply embedded, z/B is large. The overall normal effective stress at the level of the grid can be estimated from the depth and density of overlying soil. For the case of dry sand $\sigma_z' = \gamma z = \sigma_n'$

For shear on plane reinforcement surfaces, the shear stress acting on the reinforcement is usually expressed as a function of the normal effective stress acting between the soil and the reinforcement. The bearing stress acting on a grid may also be conveniently expressed as a function of this same normal effective stress. The problem is then reduced to the determination of the relationship between the effective bearing stress on the grid σ_b' and the overall normal effective stress in the surrounding soil σ_n', Fig 12b.

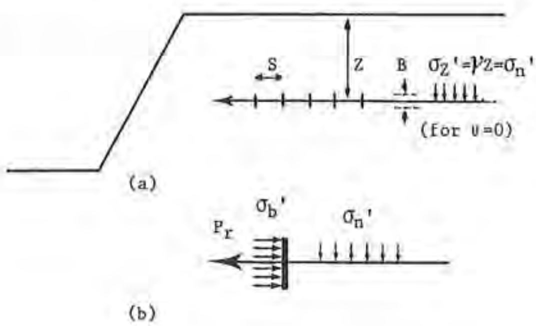

Fig.12. Definitions for bearing stresses on a reinforcement grid.

Theoretical estimates for bearing stresses

Rowe (1982) presented his results for anchors in a chart form to allow hand calculation of anchor capacity. Rowe's results can be in the form below for deeply embedded anchors,

$$\frac{\sigma_b'}{\sigma_n'} = F_\gamma' \qquad (9)$$

For grids the thickness B is typically small compared to the depth of embedment z. The value F_γ' takes account of the influence of soil dilatancy, anchor roughness and initial stress state in the soil.

Rowe's charts cover a range of soil friction angles 5° to 45°, with soil dilation angle ranging from 0 to Ø in each case. Anchor embedment z/B is in the range 1 to 8. Rowe suggests that the effect of anchor roughness and initial stress state for deeply embedded anchors can be neglected with a loss of accuracy less than 10%.

Two curves have been calculated from Rowe's (1982) charts, Fig. 13. These give a relationship between the soil bearing stress ratio σ_b'/σ_n' and the friction angle Ø for deeply embedded bearing surfaces. The curves are for the case of no dilation υ=o, and for soil dilating during shear according to the stress dilatancy flow rule assuming a critical state friction angle ϕ_{cv} = 32.5°, Rowe (1962).

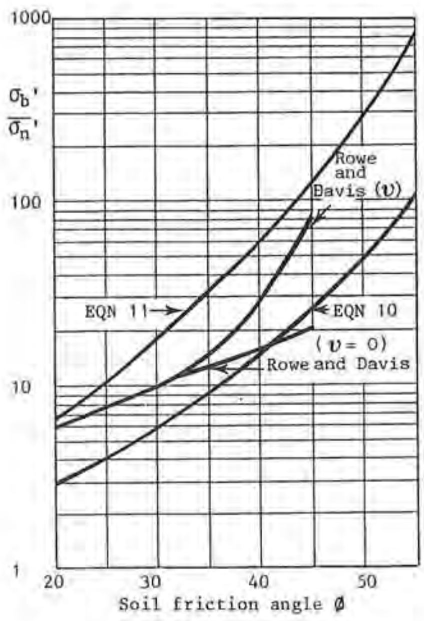

Fig.13. Theoretical relationships between bearing stress and soil friction angle.

Low bearing pressures on deep footings have been associated with a punching failure mode in the soil. The stress characteristic net and boundary stress conditions shown in Fig. 14 are suggested to provide a lower estimate of the bearing stresses on reinforcement grid members. In this case $\sigma_n' = \gamma z$, and the relationship,

$$\frac{\sigma_b'}{\sigma_n'} = e^{(90°+\phi)\tan\phi} . \tan(45°+\frac{\phi}{2}) \quad (10)$$

Equation 10 is shown plotted in Fig. 13 and gives lower values for σ_b/σ_n' to those derived by Rowe & Davis (1982).

When a grid is acting in soil like a perfectly rough sheet, the overall orientation of the principal axis of compressive stress in the soil adjacent to the reinforcement would be significantly inclined to the vertical. In compact granular soils the overall horizontal effective stress in the soil adjacent to the reinforcement may often approximately equal the overall vertical effective stress.

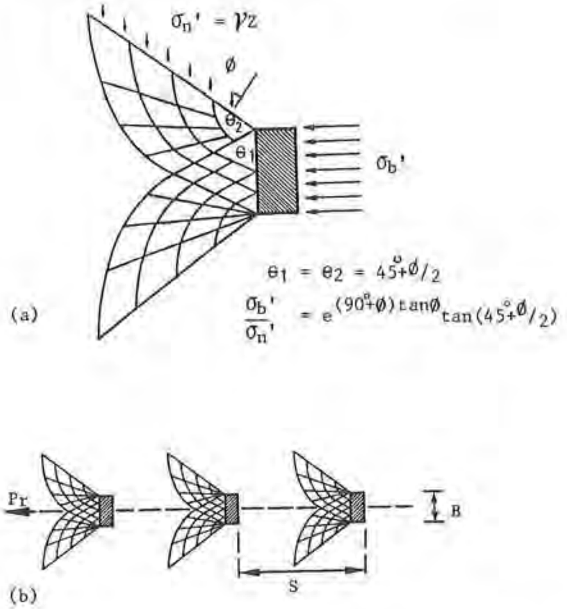

Fig. 14. Boundary conditions for bearing stresses on grid reinforcement during punching shear. Drawn for the case $\phi = 35°$.

An upper estimate of grid bearing stresses can be found by taking the conventional stress characteristic field for a footing (Prandtl (1921) & Reissner (1923)) rotated to the horizontal and a horizontal boundary stress in the soil $\sigma_h' = \sigma_v' = \sigma_n'$. The relationship between the grid bearing stress and the overall normal effective stress in the soil would then be given by the classical expression,

$$\frac{\sigma_b'}{\sigma_n'} = e^{\pi \tan\phi} . \tan^2(45°+\frac{\phi}{2}) \quad (11)$$

Equation 11 is shown plotted in Fig. 13 and gives higher values for σ_b'/σ_n' to those derived by Rowe & Davis (1982).

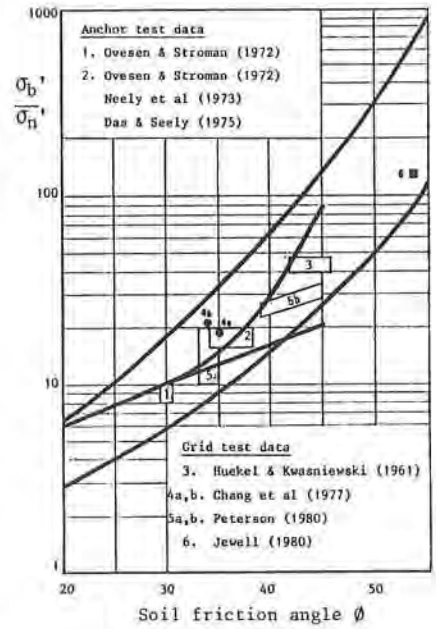

Fig. 15. Comparison of test results with predicted values of bearing stress.

Comparison with experimental bearing stresses

The anchor test results summarised by Rowe & Davis (1982) have been extrapolated to the case of deep embedment and are shown plotted in Fig. 15

Four additional sets of data from tests on grid reinforcement have been plotted, Fig. 15.

The results of Hueckel & Kwasniewski (1961) are from pullout tests on short lengths of grid embedded in a body of sand and distant from rigid boundaries. Chang et al (1977) and Peterson (1980) conducted pullout tests on grids, both on a relatively large scale. Two soils were used in both investigations.

Large direct shear tests with a reinforcement grid inclined across the central plane to reinforce the soil were conducted by Jewell (1980). The results of a series of tests at low stress level on dense sand have been used to derive the data point shown.
Although the spread and variability of the test results is large, the agreement with the theoretical predictions is encouraging. All the data are bounded by the lower and upper predictions given by equations 10 and 11 respectively, which is a satisfactory finding.

Theoretical expressions for bond strength

It is convenient to express the bond strength for grid reinforcement in terms of the total surface are a of the grid A_r. The bond strength can then be given as a bond coefficient multiple f_b of the angle of friction for the soil, thus

$$f_b \tan\phi = \alpha_s \tan\delta + f_{bearing} \tan\phi \qquad (12)$$

The first term represents the contribution from soil shearing stresses and the second term the soil bearing stresses. Dividing equation (12) by $\tan\phi$ gives a general expression for the bond coefficient,

$$f_b = \alpha_s \frac{\tan\delta}{\tan\phi} + f_{bearing} \qquad (13)$$

with the limiting condition $f_b < 1.00$.

If a grid were to act like a fully rough sheet through bearing stresses alone, so that $f_{bearing} = 1.00$, then the ratio of bearing member thickness B to spacing S would be given by an expression.

$$2S\sigma_n' \tan\phi = \alpha_b B \sigma_b' \qquad (14)$$

This is illustrated in Fig. 16. Rearranging,

$$(S/_B)_\phi = \frac{\sigma_b'}{\sigma_n'} \cdot \frac{\alpha b}{2\tan\phi} \qquad (15)$$

where $(S/B)_\phi$ is the spacing required just to give a fully rough case from bearing stresses only.

For a grid with a greater bearing member spacing, the bond strength derived from bearing stresses would be proportionally lower,

$$f_{bearing} = \frac{(S/B)_\phi}{S/B} \qquad (16)$$

Manipulating equations (15) and (16) gives the expression for the coefficient of resistance due to bearing,

$$f_{bearing} = \frac{\sigma_b'}{\sigma_n'} \frac{B}{S} \frac{\alpha_b}{2\tan\phi} \qquad (17)$$

The coefficient of bond strength for a reinforcement grid in soil can now be written in a general form, using equations (13) and (17), as,

$$f_b = \alpha_s \frac{\tan\delta}{\tan\phi} + \frac{\sigma_b'}{\sigma_n'} \frac{B}{S} \frac{\alpha_b}{2\tan\phi} \qquad (18)$$

All the parameters describing the bond strength of grid reinforcement in equation 18 can be simply determined except, perhaps, the value σ_b'/σ_n'. The data plotted in Fig. 15 indicate a value of σ_b'/σ_n' intermediate to the values given by equations (10) and (11).

The ratio σ_b'/σ_n' may be measured directly in a pullout test. Pullout tests would be best carried out with a relatively short length of grid reinforcement embedded in soil remote from rigid boundaries. The grid bearing members should ideally be spaced widely to ensure that the full bearing stress develops on each one if a value σ_b'/σ_n' is required. Otherwise the pullout test result can be used directly to estimate the bond coefficient for the grid.

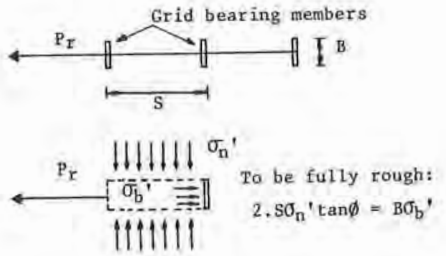

Fig.16. Basic definitions for a grid and the defining equation for the fully rough case.

Further calculations of bearing stresses

Numerical values for the ratio of bearing member spacing S to thickness B to give a fully rough grid from bearing alone may be estimated theoretically by combining equations (10) and (11) with equation (15), to give upper and lower estimates. These are shown plotted in Fig. 17, together with the logarithmic average of the two curves.

Data from grid pullout tests, and unit cell shear box tests, are shown plotted on Fig. 17 together with the value of the coefficient of reinforcement bond due to bearing. The data confirm the theoretical prediction that for values of S/B below the lower curve the grids should be fully rough, $f_{bearing} = 1.00$, and above the lower curve the roughness should decrease with increasing values S/B.

The data may also be plotted in the form suggested by equation (16), as shown in Fig. 18. The values of $f_{bearing}$ and σ_b'/σ_n' were directly back analysed from the pullout tests allowing $(S/B)\phi$ to be calculated from equation (15) to give the plotting point. The data are modelled well by the theoretical prediction.

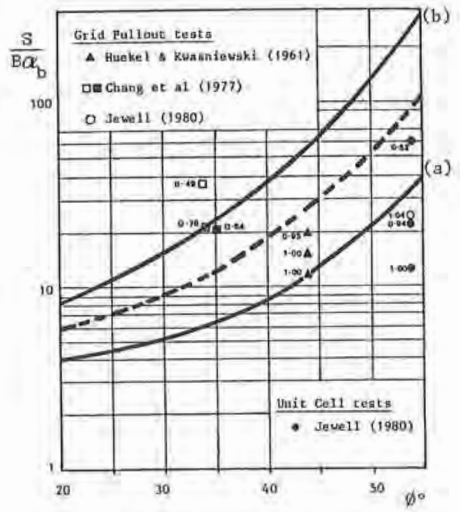

Fig.17. Lower (a) and Upper (b) predictions of $S/_B$ to give fully rough bond. Test values of f_b given next to data points.

Influence of soil particle size

Soil particle size is likely to affect bond strength in a similar way to direct sliding resistance described earlier. So, unless the average particle size is the same magnitude as the minimum aperture width, larger particles are likely to improve bond strength.

There are no test data for the influence of soil particle size on bond strength for a grid. As long as the combination of grid and soil meets the criteria specified for direct sliding.

$$\frac{\text{Minimum Aperture Width}}{\text{Average Soil Particle Size}} > 3 \qquad (7\ \text{bis})$$

then the value of maximum bond coefficient calculated from equation (18) should provide a reasonably conservative value for design.

For welded bar grids, the contribution to bond strength from shear on the plane reinforcement surfaces may typically be less than 10%. Designers may choose to ignore this contribution to bond strength when selecting a grid geometry that will act like a fully rough sheet in soil, f_b=1.00.

PORE WATER PRESSURES

The expressions for direct sliding resistance and bond strength have been derived in terms of an effective normal stress between the soil and the reinforcement grid. The magnitude of these coefficients is independent of the value of pore water pressure. The overall magnitude of stress resisting direct sliding, and bond stress giving axial reinforcement force, would however be directly reduced by pore water pressures.

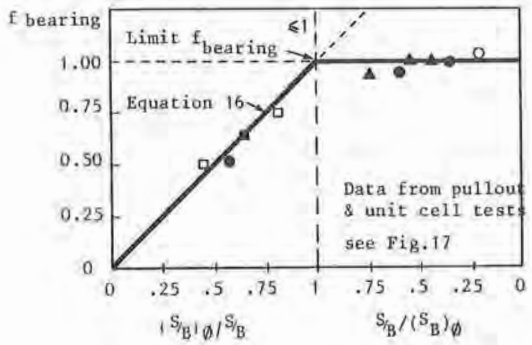

Fig.18. Relationship between the coefficient of bond due to bearing and grid geometry.

CLAY SOILS

The resistance to direct sliding and the bond strength for reinforcement grids in clay soils under drained loading conditions should be predicted from the equations given in the paper, if appropriate values of drained effective friction angle are used. Until there is data on the performance of grids in clay soils, it is recommended that direct measurements of sliding resistance and bond strength be made to select design values.

The case of clay reinforced soils subject to rapid undrained loading conditions has not been considered in the paper. Both laboratory and field measurements will be required to select design values for grids reinforcing clay in undrained loading.

DESIGN EQUATIONS

The coefficient of direct sliding resistance f_{ds} given by equation (2) applies to soil sliding over a continuous horizon of grid reinforcement.

In the practical case of reinforcement grids of width w_r spaced horizontally at s_h, the overall coefficient of direct sliding for use in a limit equilibrium analysis would be,

$$\Delta_{ds} = 1 - \frac{w_r}{s_h}(1-f_{ds}) \qquad (19)$$

The maximum value of axial force that may be generated by bond in a grid element of width w_r and length L_r subject to a normal effective stress σ_n', would be

$$\frac{(P_r)max}{2.L_r w_r.\sigma_n'} = f_b.\tan\phi \qquad (20)$$

MEASUREMENT OF VALUES FOR DESIGN

The coefficient of resistance to direct sliding of a reinforcement grid in soil can be measured simply in a laboratory direct shear test. Alternatively, if the angle of skin friction between the soil and the grid reinforcement material is known a value of peak direct sliding resistance for design can be estimated from equation (2) using $\alpha_{ds} = \alpha_s$.

The coefficient of bond strength for grid reinforcement can be measured using a pullout test. To make use of equation (18), the pullout test should be carried out on a sample of the reinforcement grid with widely spaced bearing members to ensure that the full value of bearing stress is measured. The measured value σ_b'/σ_n' would be used in equation (18) with the design ratio S/B for the grid to estimate the bond coefficient.

Design at large strain

When using relatively extensible reinforcement in soil, equilibrium conditions may require relatively large soil strains to occur. Appropriate values for direct sliding resistance and bond strength may be calculated from equations (2) and (18) using large strain values of ϕ, δ and σ_b'/σ_n'.

CONCLUSIONS

The complex interaction between soil and reinforcement grids has been radically simplified in order to provide a framework for the understanding and the interpretation of laboratory and field measurements.

Equations have been derived to evaluate the resistance to direct sliding of soil over a reinforcement grid embedded in soil, and bond strength for the grid. These allow for the influence of particle size to be included.

The conclusions drawn should be viewed in the context of the rapidly developing understanding of reinforced soil. As our knowledge increases, allowing a more sophisticated understanding of soil grid interaction, the simplified approach adopted in this paper may be improved.

The main conclusions drawn in the paper are as follows.

1. Three mechanisms of interaction between soil and grid reinforcement have been identified as,

   a. soil shearing over plane reinforcement surface areas,
   b. soil bearing on grid reinforcement bearing surfaces, and
   c. soil shearing over soil through grid apertures.

2. Examination of these show that mechanisms 1a and 1c govern the resistance to direct sliding of soil over grid reinforcement.

3. The relative size of the soil particles and grid apertures also affects direct sliding resistance. When coarse particles interlock with a grid, the resistance to direct sliding increases and can achieve values close to the full shear resistance of the soil alone.

4. Bond strength for grid reinforcement is governed by mechanisms 1a and 1b. The high ratio of bearing stress to normal effective stress in the soil makes a grid effective for bonding with soils, particularly with low friction angles.

5. Two equations have been presented which give values for soil bearing stresses on grid reinforcement Fig.15. These are supported by the available experimental data. However, the bearing stress on grid members is likely to vary depending on several other factors besides the soil friction angle and a range of results should be anticipated.

6. For grid reinforcement to develop a similar bond to a rough sheet in compact granular soils, the ratio of bearing member spacing to thickness is likely to be in the range,

   $S/B \simeq 10$ to 20

7. Similar to the case of direct sliding resistance, the relative size of the soil particles and the grid apertures may provide an increase in bond strength when coarse particles interlock with the grid and rest directly on the bearing members. However the bond strength is never expected to exceed the shear strength of the soil alone.

ACKNOWLEDGEMENTS

Work from several sources has been collected in this paper. Data from element tests have been reported which are from research by R A Jewell at Cambridge University sponsored by the Science and Engineering Research Council (SERC) and Binnie & Partners. This work is being continued at Oxford University under SERC sponsorship by G.W.E. Milligan and M. Dyer, whose photoelastic measurements have helped elucidate the fundamental mechanisms described. The measurements of direct sliding resistance were made by R W Sarsby and C Marshall at the Bolton Institute of Higher Education during research sponsored by Netlon Limited, and guided by D.D. Dubois who developed laboratory techniques for direct sliding measurements at Queen's University, Belfast. The theoretical studies were carried out by R A Jewell for the cooperative research project into Civil Engineering applications of polymer grids sponsored by the SERC and Netlon Limited. The authors gratefully acknowledge the sponsorship which has supported the work, and the contributions of colleagues too numerous to name individually.

REFERENCES

Arthur, J.R.F., Dunstan, T., Al-Ani, Q.A.J.L. and Assadi, A. (1977). Plastic deformation and failure in granular media. Geotechnique 27, No.1 53-74.

Bhudu, M. (1979). Simple shear deformation of sands. Ph.d Thesis University of Cambridge.

Chang, J.C., Hannon, J.B. and Forsyth, R.A. (1977). Pull resistance and interaction of earthwork reinforcement and soil. Transportation Research Record 640, Washington, D.C.

Das, B.M. and Seeley, G.R. (1975). Pullout resistance of vertical anchors. J. Geotech, Engng Div. Am.Soc.Civ. Engrs 101, GT 1.87-91.

Forsyth, R.A. (1978). Alternative earth reinforcements, Symposium on Earth Reinforcement ASCE.

Hueckel, S.M., and Kwasniewski, J., (1961). Scale model tests on the anchorage values of various elements buried in sand. Proc. 5th ICSMFE Paris.

Jewell, R.A. (1980). Some effects of reinforcement on soils. Ph.D Thesis. University of Cambridge

Kerisel, J. (1961). Deep foundations in sands. Variation of ultimate bearing capacity with soil density, depth, diameter and speed. Proc 5th ICSMFE Paris

Neely, W.J., Stewart, J.G. and Graham, J. (1973). Failure loads of vertical anchor plates in sand. J. Soil Mech. Fdns Div. Am. Soc.Civ Engrs 99 SM9 Sent 669-685

Netlon Limited (1984). Test methods and physical properties of 'Tensar' Geogrids. Technical publication.

Ovesen, N.K. and Stroman, H. (1972). Design methods for vertical anchor plates in sand. Proceedings of speciality conference on performance of earth at earth supported structures, pp. 1481-1500. New York: American Society of Civil Engineers.

Peterson, L.M. (1980). Pullout resistance of welded wire mesh embedded in soil. M.Sc. Utah State University

Potyondy, J.G. (1961). Skin friction between cohesive granular soils and construction materials. Geotechnique 11, No. 4, 339-353

Prandtl, L., (1921). "Uber die Eindringungsfestigkeit platisher Baustoffe und die Festigkeit von Schneiden." Zeitschrift fur Angewandte Mathematik und Mechanik, 1: 1, 15-20.

Reissner, H., (1924) "Zum Erddruckproblem." Proc. First Intern. Conf. Applied Mech., 295-311, Delft.

Roscoe, K.N.. (1970). The influence of strains in soil mechanics. Geotechnique 20, No.2, 129-170.

Rowe, P.W. (1962). The stress dilatancy relation for static equilibrium of an assembly of particles in contact. Proc. Roy. Soc. A, 269, 500-527.

Rowe, R.K. and Davis, E.H. (1982). The behaviour of anchor plates in sand. Geotechnique 32, No. 1, 25-41.

Schlosser, F., Jacobsen, H.M., and Juran, I. (1983). Soil reinforcement. General report. Proc. 8th Eur. Conf. Soil Mech. Fndn. Engng., Vol 3, Helsinki.

Schlosser F. and Juran, I. (1979). Design parameters for artificially improved soils. General report. Proc. 7th Eur. Conf. Soil Mech. Fndn. Engng., Vol 5, Brighton.

Vesic, A.B. (1963). Bearing capacity of deep foundations in sand. Highway Research Record No. 39. National Research Council, Washington. D.C.

NOTATION

A_r	$(=W_r.L_r)$ total plan area of grid.
B	thickness of bearing members
D_{50}	the effective particle size which corresponds to 50% passing on the grain size diagram
$f_{bearing}$	coefficient of reinforcement bond due to bearing
f_b	coefficient of reinforcement bond
f_{ds}	coefficient of resistance to direct sliding
F_γ'	factor for bearing on anchors (Rowe & Davis 1982)
L_r	length of reinforcement available for bond
P_r	axial reinforcement force
S	spacing between bearing members
s_v	vertical spacing between reinforcements in a reinforcement layout
s_h	horizontal spacing between reinforcements in a reinforcement layout
W_r	width of reinforcement
z	depth of embedment
α_b	fraction of grid width over which bearing surface extends
α_{ds}	fraction of grid surface area that resists direct shear with soil
α_s	fraction of grid surface area that is solid
$(1-\alpha_s)$	fraction of grid surface area that is aperture
γ	unit weight of soil
δ	angle of friction between soil and the reinforcement surface
Δ_{ds}	design overall coefficient for direct sliding
ν	angle of soil dilation
ϕ	angle of friction of soil
ϕ_{ds}	angle of friction of soil in direct shear
ϕ_{cv}	angle of friction of soil at constant volume
σ_n'	normal effective stress between soil and reinforcement
σ_b'	effective bearing stress between soil and reinforcement

Use of geogrid properties in limit equilibrium analysis

This paper provides guidance on the choice of soil, geogrid and soil-geogrid interaction properties that should be used in limit equilibrium analysis of geogrid reinforced soil structures. It suggests that as little experience exists for the evaluation of lumped factors of safety in design, partial factors of safety should be used. The material properties to which these partial factors should be applied and the reasoning for each of them is given. Finally, the differences between overall strains, and so deformations, at working conditions and those inherantly assumed in limit equilibrium designs are discussed.

A. McGown, *University of Strathclyde,*
N. Paine, *Binnie and Partners,* and
D. Dubois, *Netlon Ltd*

INTRODUCTION

As with any civil engineering construction, it is necessary to ensure that a reinforced soil structure performs satisfactorily during its lifetime, under all reasonably foreseeable circumstances. To do this, two distinct phases must be considered:

(i) The construction stage.

(ii) The post-construction stage.

Additionally, it is necessary to ensure that during each phase, the structure performs without exceeding the following two limiting conditions:

a) A limiting equilibrium condition, at which one or more of the materials within the structure ruptures.

b) A limiting serviceability condition, at which the structure deforms more than is acceptable.

To accomplish this, an appropriate means of predicting the behaviour of the structure must be identified and the operational properties of both the soil and the reinforcement material established. Additionally, soil structures incorporating relatively extensible reinforcements, such as geogrids, are strain controlled systems, McGown et al (1978), hence there must be strain compatibility between the soil and the reinforcements at all times. Thus the strength parameters for the reinforcements must be measured over the same range of strains as can occur in the soil.

Following the choice of design method and material properties, factors of safety need to be applied to allow for the inadequacies of the design method, extreme loads and variations in soil and reinforcing material properties. A single lumped factor of safety to allow for all these is the simplest approach, but at this stage in the development of soil reinforcement technology, little experience exists for evaluation of the magnitude of such a factor. The concept of partial factors of safety can be used to concentrate attention on the various components of reinforced soil which, taken together, require a margin for safety.

In the following sections of this paper, alternative methods of design are discussed, the approach to the selection of appropriate material properties are identified for limit equilibrium designs and the parameters to which partial factors of safety should be applied are identified, together with the reasoning for the need of these factors. Also guidance is given on the estimation of overall deformations of geogrid-reinforced soil structures, in order to assess limiting serviceability conditions.

DESIGN METHODS

The available methods of analysis for reinforced soil systems can be classified as purely empirical methods, methods based on back analysis of laboratory models or field trial structures and methods based on the analysis of the internal stresses of the system. These latter methods may be categorised further into methods based on numerical techniques, such as the finite element techniques of Romstad et al (1976), Al-Hussaini and Johnson (1978) and Andrawes et al (1982), methods based on behavioural models of working conditions, such as the "Energy" method of Osman (1977) and limit equilibrium methods, such as those of Schlosser and Vidal (1969), Schlosser (1972), Lee et al (1973), Broms (1977) and Murray (1978). The finite element techniques are attractive as, in principle, they can model the stress and strain conditions throughout the reinforced system. However, these techniques are not yet commonly used in design offices, the most widely used being limit equilibrium methods. This paper therefore deals with the selection of geogrid data for use in designs employing limiting equilibrium methods of analysis.

MATERIAL PROPERTIES

The material properties used in designs employing limit equilibrium methods of analysis for soil-geogrid systems, are the strengths of the soil and the geogrid reinforcements together with a parameter to describe their surface interaction. The strength of the soil, under various conditions of drainage, is most commonly measured using the triaxial or shear box apparatuses, although many other methods are available. McGown et al (1984) have shown that rapid loading creep testing of geogrids allows their load-strain-time behaviour to be quantified and Jewel et al (1984) have shown that the shear box is an effective method of quantifying soil-geogrid interaction. Just as important as the method of testing, however, is the presentation and choice of the data from these tests.

In order to ensure strain compatibility between the soil and the geogrid at all times, the likely strain levels mobilised at the limiting equilibrium condition must be known. Most reinforced soil structures are built with compacted granular soils and their axial strains at peak strength are associated with lateral tensile strains of 8 per cent at most. Although for dense sands, many investigators have shown that the lateral tensile strains at peak strength (stress ratio), in axial compression may often be less than 6 per cent, Jewell (1980). Thus if peak strength parameters are used for the soil, the forces in the geogrid inclusions lying in or close to the directions of principal tensile strains, must be limited to the forces developed at corresponding strain levels.

Although once passed their peak strength, compacted granular soils reduce their strength with continuing straining, they eventually attain a constant volume at which strength does not vary with continued straining, Fig. 1

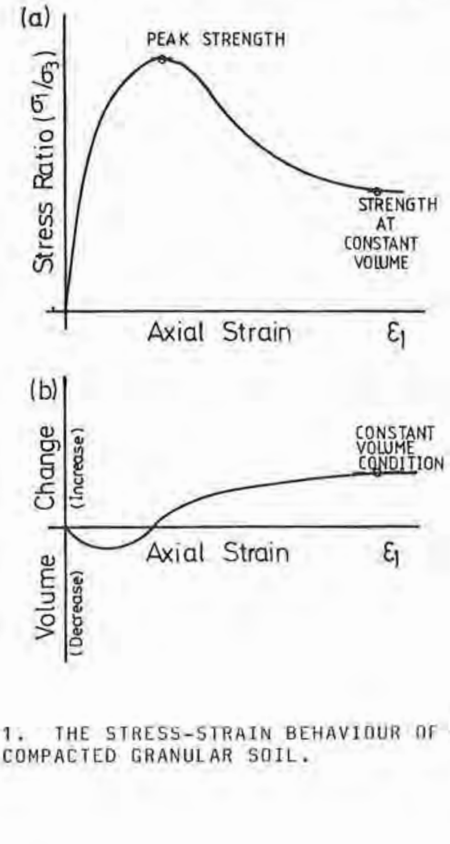

FIG. 1. THE STRESS-STRAIN BEHAVIOUR OF A COMPACTED GRANULAR SOIL.

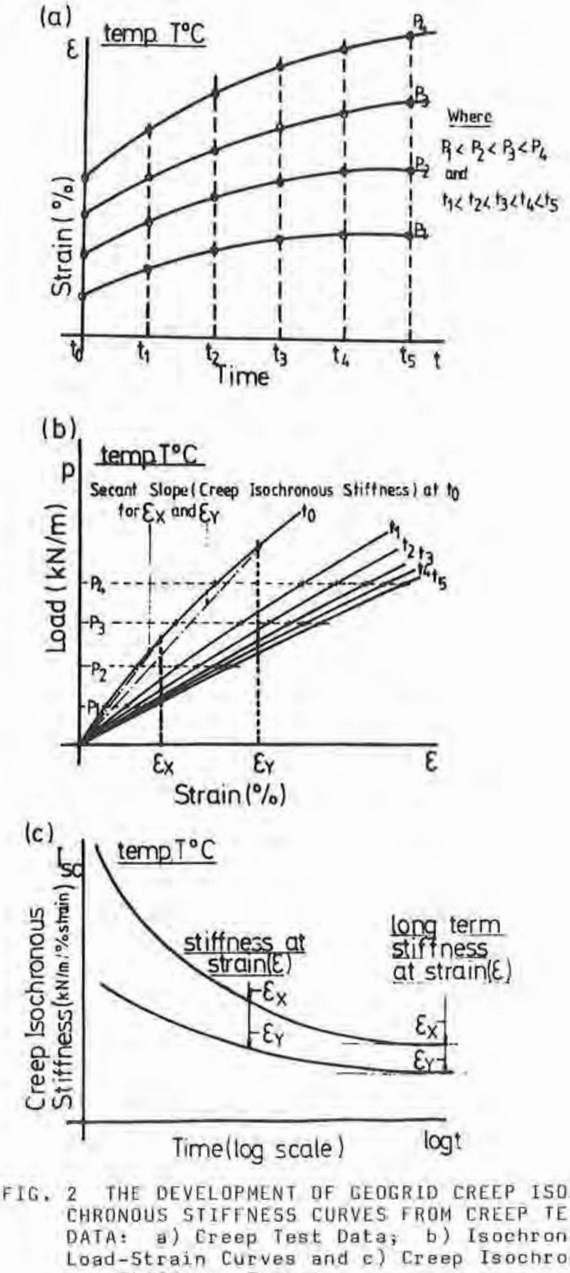

FIG. 2 THE DEVELOPMENT OF GEOGRID CREEP ISOCHRONOUS STIFFNESS CURVES FROM CREEP TEST DATA: a) Creep Test Data; b) Isochronous Load-Strain Curves and c) Creep Isochronous Stiffness Curves.

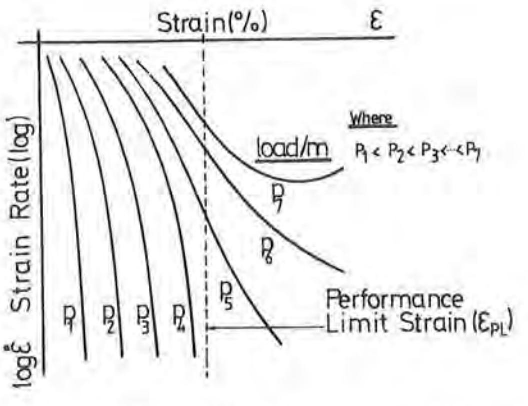

FIG. 3. PLOT OF STRAIN AGAINST LOG. STRAIN RATE TO DETERMINE THE PERFORMANCE LIMIT STRAIN.

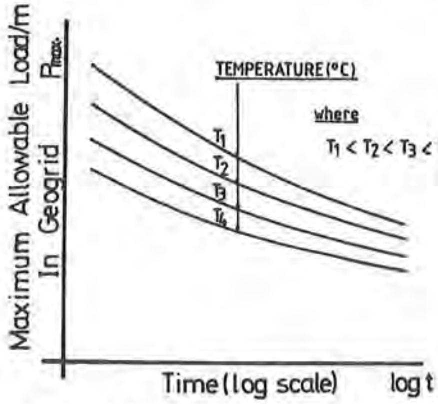

FIG. 4. PLOT OF MAXIMUM ALLOWABLE LOAD/m AGAINST TIME FOR DIFFERENT TEMPERATURES.

Thus strains beyond those required to mobilise peak strength need not immediately induce conditions of limiting equilibrium. As the soil strains and its strength reduces from its peak value to that at constant volume, so the geogrid mobilises more force and overall the soil-geogrid system may remain in equilibrium. Only when lateral tensile strains in the soil induce strains in the geogrid which cause it to approach rupture, will a limiting equilibrium condition be reached. Thus for geogrids within compacted granular soils, the most likely limiting equilibrium condition occurs when the soil has strained beyond its strain to peak strength and has reached a state of constant volume. The geogrid may then be approaching rupture. Hence for designs employing limit equilibrium methods for soil-geogrid systems, the mobilised strength of compacted granular soils should be taken as their angle of friction at constant volume, (ϕ_{cv}).

The data from rapid loading creep tests on geogrids may be replotted as isochronous load-strain plots, as shown in Figs. 2(a) and (b).

The secant slopes of these isochronous load-strain curves for various levels of strain are termed the "Creep Isochronous Stiffnesses" and should be plotted against time as in Fig. 2(c), for various operational temperatures, with zero time in each plot taken as the time to reach half full load, McGown et al (1984). Thus for strains up to rupture of the geogrid, the operational load at any time and temperature is taken as the product of the strain in the geogrid and the appropriate isochronous stiffness.

In order to identify the maximum load that can safely be applied to the geogrid, the maximum strains that may be induced without risk of rupture must be identified for various temperatures. These maximum strain values are termed "Performance Limit Strains", McGown et al (1984), and are evaluated from plots of cumulative strain against the logarithm of strain rate at different temperatures, after Wilding and Ward (1978), Fig. 3. Knowing these, then the maximum allowable load in the geogrid at any time and temperature is obtained by taking the product of the appropriate performance limit strain and creep isochronous stiffness, as shown in Fig. 4.

The soil-geogrid interlock data from the shear box tests may be presented as equivalent soil-geogrid friction angles (δ). It is also convenient to state these data as soil-geogrid interaction coefficients (α), which are the ratios of the equivalent soil-geogrid friction angles to the soil friction angles. In each case, the density of the soil must be indicated as the efficiency of soil-geogrid interlock is not independent of soil density, Jewell et al (1984). Also the soil-geogrid interaction coefficient is not necessarily the same for peak and constant volume soil friction angles, often approaching unity for the latter. Thus in many designs employing limit equilibrium methods for soil-geogrid systems, the soil-geogrid friction angle may be taken to be that for the soil at constant volume where the assumed shear failure surface passes along the geogrid, but in areas away from the failure surface it may be taken as an appropriate fraction of the peak soil friction angle, for example when calculating anchorage lengths.

PARTIAL FACTORS OF SAFETY

The basis of designs employing limit equilibrium methods of analysis, for soil-geogrid systems, is the establishment of the out-of-balance force that exists in the structure at limiting equilibrium conditions. To calculate this, the loads applied and the mobilised soil strength must be estimated, then the forces that should be generated in the reinforcements may be established. Partial factors of safety are employed at each part of the calculation process in order to account for factors such as variability of loads and materials, durability of materials, lack of accuracy of the design model and influence of construction methods.

The loads applied to reinforced soil structures may either be dead or live loadings. For dead loadings a high degree of confidence can be placed on the estimation of the largest expected values of these hence it is generally possible to apply a partial factor of safety of unity. The partial factors of safety to be applied to live loadings vary with the purpose of the structure but is generally encompassed in the choice of the worst combination of load conditions that can be envisaged.

As stated previously, it is necessary for soil-geogrid systems to ensure that strain compatibility exists between the soil and the geogrid. Thus for compacted granular soils, their limiting strength is likely to be their strength at large strains, i.e. constant volume (ϕ_{cv}) Fig. 1. As this can be measured relatively simply with a high degree of confidence for most granular soils, then it is often possible to use a partial factor of safety of unity on the soil strength. Thus for most types of limit equilibrium analysis, the angle of friction at constant volume (ϕ_{cv}) can be used directly in calculations.

The forces that can safely be generated in the geogrid reinforcement depend on the maximum load in the grid not causing rupture and on there being sufficient anchorage lengths away from the critical shear surface within the structure. Thus partial factors of safety need to be considered for both the strength of the geogrid and the soil-geogrid interaction coefficient used in the design.

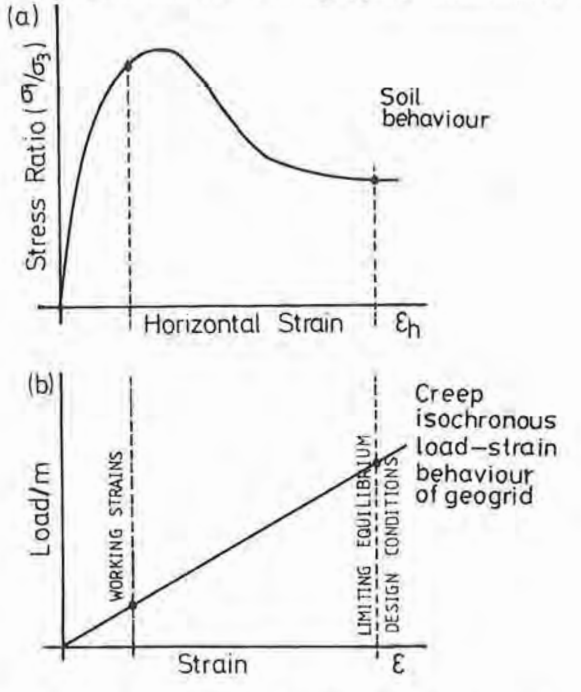

FIG. 5. THE POSSIBLE DIFFERENCE IN WORKING STRAINS AND THE STRAINS AT LIMITING EQUILIBRIUM CONDITIONS ASSUMED IN DESIGNS.

The strength of the geogrid that can be taken in the design calculations is the product of the operational strain and the appropriate isochronous stiffness of the material. The value of isochronous stiffness chosen should not only take account of the operational temperature and design life of the structure but also of the variability of the production materials. C.I.R.A. Report No. 63 (1977) suggests that in order to do this for construction materials, the strength used should be the "characteristic strength", defined as the strength which has a 95 per cent probability of being attained.

Partial factors of safety should be applied to this value of production materials characteristic strength which will usually be provided by the manufacturer. For geogrids the inadequacies of the design models, particularly the assumption that pure creep occurs from the time of achieving half full load with no account taken of the possibility of load relaxation, requires a partial factor to be applied. The possibility of variations occurring during construction in the vertical spacing and lengths of reinforcement layers must be similarly allowed for. Additionally the possibility of site damage to the geogrid during compaction and the possible subsequent deterioration of the material with time must all be allowed for by applying a partial factor of safety to the strength of the geogrid. These various partial factors may be lumped together and should then be related to the type of soil in which the geogrid is compacted, to the method of construction and to the design lifetime of the structure involved.

The possibility of applying a partial factor of safety to soil-geogrid interaction should also be considered. In many forms of reinforced soil structures, the soil-geogrid interaction does not dominate the stability calculations and the assumption that the soil-geogrid friction angle is that of the soil is thus often satisfactory.

Where the depth of the geogrid reinforcement is less than one or two metres below the surface, a considerable length of reinforcement may be necessary to anchor the force that can be safely taken in the geogrid. In such cases a partial factor of safety might be applied to soil-geogrid friction angle. However, in practice the need to mobilise the full allowable force in a shallow layer of reinforcement normally arises from the possibility of a deep shear surface developing, which intersects several other reinforcing layers. Practical geogrid reinforcing layouts provide excess capacity and any apparent shortfall in anchorage near the surface will therefore usually be more than compensated for at depth.

ESTIMATE OF OVERALL DEFORMATIONS

When partial factors of safety for uncertainties in design models, site damage, inaccuracies in construction and long term durability have been applied to the production materials characteristic strength and this is used in conjunction with the soil angle of friction at constant volume and its related soil-geogrid friction angle, the equilibrium strains at working conditions are likely to be much less than those assumed in the design. Indeed as indicated in Fig. 5, it is likely that the working strains will be less than the horizontal strains required to bring the soil to peak strength. For well compacted granular soils, equilibrium strains in the zone of maximum shear stresses are likely to be of the order of only 3 or 4 per cent. The distribution of forces and so strains along geogrid reinforcements is as yet not known. Measured distributions of forces and strains in reinforcements have principally been associated with metal strips. These of course rely on a surface friction stress transfer mechanism rather than interlock, and so it is possible that the distributions of force and strain along the strips will be different from those along grids. It may, however, be suggested that at working conditions the average forces and strains along the grids will be a fraction of the maximum working forces and strains. The overall working deformations of geogrid reinforcements will therefore be very small and will not approach the deformations that would develop were the strains assumed in the limitint equilibrium condition to be generated.

DISCUSSION

The paper has made clear recommendations for the selection of appropriate material properties for use in designs employing limit equilibrium analysis and for the partial factors of safety that should be used in conjunction with these. These recommendations may be summarised as follows:

1. Soil Property (Compacted Granular Soil)

$$\text{Angle of Soil Friction} = \frac{\phi_{cv}}{\gamma_S}$$

where ϕ_{cv} is the angle of friction at constant volume (large strains).

γ_S is the partial factor of safety for soil friction and is often taken to be unity.

2. Geogrid Property

$$\text{Safe working load at time (t) and temperature } (T°C) = \frac{P_{PM}}{\gamma M}$$

where P_{PM} is the production material characteristic strength at time (t) and temperature (T°C), taken as the product of the performance limit strain and the appropriate creep isochronous stiffness, (this includes an allowance for production variability).

γ_M is the partial factor of safety for the geogrid which takes account of deficiencies in the design model, site damage, construction inaccuracies and durability.

3. Soil-Geogrid Friction (Using Compacted Granular Soil)

$$\text{Angle of Soil-Geogrid Friction} = \frac{\delta}{\gamma_I}$$

where δ is usually taken to be equal to angle of soil friction.

γ_I is the partial factor of safety for soil-geogrid friction and is often taken equal to unity.

4. Applied Loads

Partial load factors may or may not be applied to dead loads and live loads depending on the nature of the loads and the structure.

For certain structures it may be necessary to undertake an analysis for both short and long term if the soil or loading conditions are likely to change with time. Nevertheless for most cases, geogrid reinforced soil structures need only be designed for limiting equilibrium conditions in the long term. The strains assumed in this design are not, however, likely to occur as equilibrium working conditions are likely to be achieved at strains less than those required to generate peak strength in the soil.

ACKNOWLEDGEMENTS

The authors wish to acknowledge that this work results from the efforts of the Soil Reinforcement Design Group set up as part of the Science and Engineering Research Councils Co-operative grant made in conjunction with Messrs. Netlon Ltd.

REFERENCES

Al-Hussaini, M.M. and Johnson, L.D. (1978). Numerical analysis of a reinforced earth wall. Proc. Sym. on Earth Reinforcement. ASCE Annual Convention Pittsburgh. 98-126.

Andrawes, K.Z., McGown, A., Wilson-Fahmy, R.F. and Mashhour, M.M. (1982). The finite element method of analysis applied to soil-geotextile systems. Proc. 2nd Int. Conf. on Geotextiles, Las Vegas 3 695-700.

Broms, B.B. (1977). Polyester fabric as reinforcement in soil. Int. Conf. on the Use of Fabrics in Geotechniques. Paris 1. 129-135.

C.I.R.I.A. Report No. 63 (1977) Rationalisation of safety and serviceability factors in structural codes. Construction Industry Research and Information Association. 226 pp.

Jewell, R.A. (1980) Some Effects of Reinforcement on the Mechanical Behaviour of Soils. PhD Thesis, University of Cambridge. (unpublished).

Jewell, R.A., Milligan, G.W.E., Sarsby, R.W. and DuBois, D.D. (1984). The interaction between soil and geogrids. Proc. Symp. on Polymer Grid Reinforcement in Civil

Engineering. Mar.

Lee, K.L., Adams, B.D., and Vagneron, J.J. (1973). Reinforced earth walls. Jour. S.M. and F.E. Div. ASCE. 99. 10. 745-763.

Murray, R.T. (1978). Design of reinforced earth walls. T.R.R.L. Int. Report 18 pp.

McGown, A., Andrawes, K.Z. and Al-Husani, M.M. (1978), Effect of inclusion properties on the behaviour of sand. Geotechnique 28. 3 327-346.

McGown, A., Andrawes, K.Z., Yeo, K.C. and DuBois, D. (1984). The Load-Strain-Time Behaviour of Tensar Geogrids. Proc. Symp. on Polymer Grid Reinforcement in Civil Engineering. Mar.

Osman, M.A. (1977). An Analytical and Experimental Study of Reinforced Earth Walls. Ph.D. Thesis University of Glasgow (unpublished).

Romstad, K.M., Herrmann, L.R., and Shen, C.K. (1976). Integrated study of reinforced earth - 1: theoretical formulation. Jour. Geot. Eng. Div. A.S.C.E. 102 GTS 457-471.

Schlosser F. (1972). La terre armee, researches et realisations. Bull. Liason. Lab. Ponts. et Chauss. 62.72-92.

Schlosser F. and Vidal H. (1969) Reinforced Earth. Bull Liason. Lab. Ponts. Chauss.41.

Wilding, M.A. and Ward, I.M. (1978). Tensile creep and recovery in ultra-high modules linear polyethylenes. Polymer.19, 969-976.

Introduction to polymer grids: report on discussion

J. E. Templeman, *Netlon Ltd*

The possible increases in tensile strength of Tensar grids (given as an illustration to the keynote speech) were further described by Prof. Sir Hugh Ford as an indication that one could proceed much further up the stiffness curve provided by Prof. Ward (paper 1.1). The practical limits for these increases were subjects of research and discussion.

Prof. Ward was encouraged by these possible improvements and stressed the need for continued development on the production process and stated that he had no doubt that polymers could be made intrinsically as stiff as glass or aluminium in large section.

The induction of increased strain hardening during the manufacturing process was explained by Prof. Ward to occur as the result of the production of chemical cross-links. Radicals are produced during the stretching process, which possibly react with other chemicals present, but in any case succeed in joining molecular chains together to form a chemical network.

Orientation improves many properties, not just strength and stiffness. In particular, it reduces the permeability to gases, so it improves chemical resistance, and it makes the material more stable, both in the sense that it has a much lower thermal coefficient of expansion, and that it has less permanent shrinkage.

In answer to a further question posed specifically on any ageing or hardening effect caused by organic agents or bacteria in the soil, Prof. Ward stated that polyethylene had been well examined by the medical community, had been found inert and not subject to biological attack, to the extent it is used in internal prostheses.

Other contributors suggested that polyethylene had been used in soil for 50 years - as cable covering and water piping - with the only real problem being one of disposal.

Studies had recently been completed on a range of pulverised fuel ash materials, to check whether any chemicals present in these chemically aggressive materials would cause deterioration of polymer grids.

None were effectively found.

Dr McGown, presenting paper 1.2 emphasised that the properties of the soil as well as the polymer grid have to be considered. Polymer grids have to be designed which are compatible with the soil, not to be too brittle, and not too extensible.

If equilibrium is attained at low strains under working conditions, and we design for failure at large strains, considerable warning will be provided before the structure fails.

We are designing a composite.

Dr Bassett agreed that we are dealing with a composite and that compatibility of strain is important, but disagreed with the use of classic limit analysis mechanisms with the reinforcement assumed to be an additional "tie force".

The parameters of a soil are not altered when we reinforce it, but the composite is restrained to behave in a different manner.

If an ordinary active retaining wall were considered purely on the basis of stresses, it was agreed that the failure mechanism would be on the basis of a wedge at 45 degrees + $\phi'/2$.

On the basis of strains, ruptures are constrained to take place eventually in the direction at right angles to the zero extension planes. These directions are related to the dilation characteristic ψ .(ψ and ϕ' are often assumed equal in "upper bound" calculations).

The stiffness of the reinforcement will control the orientations of the zero extension planes.

If the case of a reinforced wall is considered, the reinforcement is conventionally placed in a horizontal direction and the mechanism described by Jewell et al (paper 1.3) can be acceptable, - sliding on the surface of the reinforcement could occur, driven by an active wedge outside it.

This is similar to a concrete block sliding on a layer of weak material left in the concrete, it does not do justice to reinforced earth.

If the soil lying parallel to the grid is strained and the reinforcement locked into the soil system then displacements in the soil will cause the grid to be pulled in two directions. It is therefore not clear whether or not shear tests or pull out tests had much relevance with what happened in the composite.

If the grid will remain unslipping with respect to the soil, then it is the compatibility of strain in the horizontal, or in the reinforcement direction, that is important.

If we deal with the compatibility of strain then the zero extension planes must be moved and the potential rupture plane at right angles to these will also be in a different orientation (Fig. A).

The behaviour of the reinforced earth wall is therefore a system in which there is a much modified failure mechanism with different slip planes operating.

In the limit when the reinforcement will not strain at all the mechanism for failure becomes very different from the classic active case as we normally understand it.

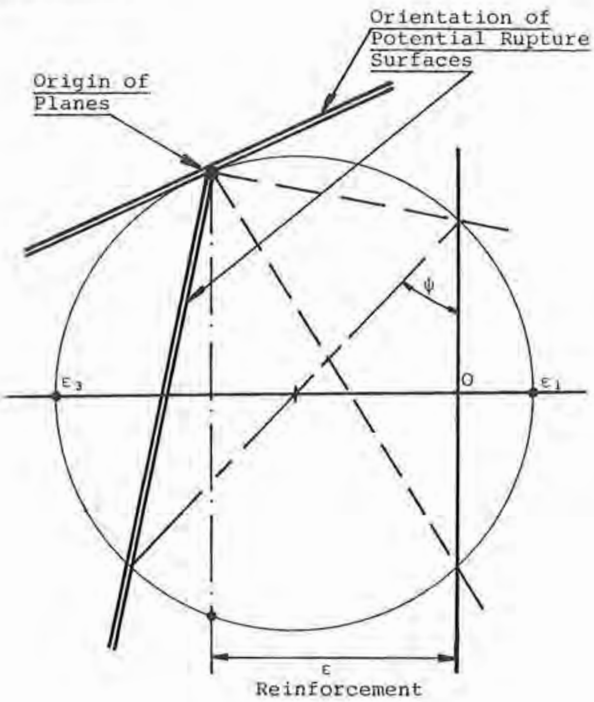

Fig. A. Mohr's circle of strain

The value of ϕ' would still be valid but the σ_h' and σ_v' values would have to agree with the principal stress directions as re-orientated to comply with strain compatibility.

In reinforced earth therefore, there is a rotation of the principal stress and strain directions, which must alter our whole concept of how this system works. As the strain in the soil and the strain in the grid are comparable with each other then the grid will only carry the amount of stress that the soil strain will generate in it, and the resulting change will be an increase in and a rotation of principal directions.

Dr Bassett emphasised that it was comparative strain and compatible strain that would define the whole ability to produce reinforced earth and therefore that reinforcement stiffness was a significant parameter.

In discussing paper 1.3, Dr Jewell expressed disagreement with Dr Bassett in:-

a) Relevance of the pull out test.

The pull out test was performed to find the limiting value of the bond strength, so that the maximum value of the force could be calculated - assuming it to be inextensible - or in the regions near the end of the reinforcement, where forces and therefore strains are very low.

In substituting values in limit equilibrium calculations the value of force used may be governed by limiting the magnitude of tensile strain to 2% or 3% - to comply with allowable working conditions. Pull out tests were therefore considered to have relevance.

b) Overall failure modes

Internal surfaces drawn through reinforced blocks are surfaces upon which equilibrium can be estimated - by estimating the equilibrium looking at the magnitude of mobilised reinforcement across the surfaces, and the effect the mobilised force would have on shear resistance.

c) If there is no tensile strain in the direction of inextensible reinforcement, then the reinforced soil is not going to fail, and so this mechanism of failure would never be observed.

d) Looking at inextensible reinforcements in soil, if the reinforcement is in the direction of zero extension and the reinforcement bonded perfectly with the soil, you may hope to see a pattern of strain, giving a zero extension line along the reinforcement.

Caution was however advised in using uniform patterns of stress and strain to describe discontinuous phenomena in the field.

Relevant movement was required in the case of grids to generate bearing forces.

Dr Jewell advised that in the case of a Geogrid being placed at the interface between two dissimilar soils, the bond strength could be estimated as the average of the bond strengths of two soils with the Geogrid, or if a conservative value was required, then the bond strength between the Geogrid and the weaker soil should be taken.

In discussing the possible variation between the established method for calculating the effective adherence length for non-extensible reinforcement - and a method for calculating the effective adherence length for extensible reinforcement, the author suggested:-

i) Limit equilibrium equations might show that in reinforced soil, the locus of maximum force, is a consequence only of the reinforcement providing equilibrium, on all potential surfaces through the soil and that there is no one failure mechanism to which we can ascribe the presence of that locus.

ii) A procedure could be, to estimate, using soil interaction, what the maximum force could be along each reinforcement in its position in the soil increasing from the end embedded deepest in the soil, perhaps maintaining a force in the case of a rigid face, or dropping again to zero, where a loose face was used.

From the maximum force envelope, one could then use limit equilibrium calculations to calculate the mobilised value of force.

There would not be a calculation of bond length. It would simply be that each reinforcement would contribute a portion of the maximum force envelope.

iii) When extensible reinforcement was used, the maximum force and maximum force envelope will be governed by serviceability considerations in the maximum allowable tensile strain.

Answering a question relating to Paper 1.4 about the strength of the crossbars of the Geogrid, Dr DuBois explained that the development of bond stress occurred as a buttress effect on the crossbar such that the acceptance of stress, occurred by transmitting positive pressures.

The critical strength of the Geogrid must therefore be its ability to accept the tensile stresses generated by interaction along the length of the reinforcement.

Creep test values of the Geogrid had been obtained from the whole material being examined in this mode.

An alternative combination of value of ϕ and partial factor of safety was suggested, instead of the use of ϕ_{cv} and a partial factor of unity. The author explained that, in accepting there should be strain compatibility between the soil and the Geogrid, at the limiting equilibrium condition at high strain, it must be assumed that the two materials are comparable at the worst conditions.

The actual profile of the soil (Fig. 4 of Paper 1.4) was indicative of a well compacted material, and would not likely be worse in performance than the condition indicated by ϕ_{cv}.

A partial factor of safety of unity was therefore recommended for the soil in high strain condition.

PARTICIPANTS:

Professor Sir Hugh Ford FRS

Professor Ward FRS

Dr Bonaparte

Dr McGown

Dr Jones

Professor Nordal

Dr Bassett

Dr Jewell

Professor Jarrett

Dr Juran

Dr Osborn

Dr DuBois

Dr Craig

Introduction to polymer grids: written discussion contributions

Professor T. S. Ingold, John Laing Construction Ltd and Queen's University, Belfast

In Fig. 1 of paper 1.3, Jewell et al. define two failure mechanisms in granular soil, namely direct sliding of soil over reinforcement and pull-out of the reinforcement. These same mechanisms would apply in the undrained loading of saturated clay where both sliding and pull-out resistance can be expressed in terms of the undrained shear strength C_u. Direct sliding resistance can be expressed in terms of an average adhesion αC_u, where α is an adhesion factor that can never exceed unity. For a planar or thin grid this average adhesion will comprise two components. Firstly, in the clay filled apertures of the grid there will be direct clay to clay contact for which the local adhesion factor is unity. Secondly, there will be adhesion mobilised between the clay and the material of the grid for which the local adhesion factor is β. Taking the open area ratio of the grid to be ρ the average adhesion factor can be expressed by equation (1).

$$\alpha = \varrho + \beta (1 - \varrho) \tag{1}$$

To illustrate the results that can be obtained using equation (1), two grids are considered - Netlon 1168 and Weldmesh 5119. Table 1 gives grid data together with theoretical values of α from equation (1) and measured values obtained from direct shear box tests (Ingold, 1980).

Pull-out resistance T, can be evaluated using an expression in the form of equation (2).

$$T = N_c C_u \Sigma a + \beta C_u \Sigma a_s \tag{2}$$

The first term in this expression relates to the bearing force generated by transverse grid members. This is the product of a bearing factor N_c, the undrained shear strength of the clay and the sum of the areas of the grid members Σa, normal to the direction of pull-out. The second term relates to surface adhesion βC_u, generated on the sum of the surface areas Σa_s , parallel to the direction of pull-out. Equation (2) is a general expression which can be developed for a planar punched grid or a welded rod grid. For example, if the sum of the normal and parallel components of the members' lengths are Σl_n and Σl_p respectively, then for an orthogonal grid of rod of diameter D

$$T = N_c C_u D \Sigma l_n + \beta C_u \pi D \Sigma l_p \tag{3}$$

The adhesion factor α has been previously defined as the ratio of apparent surface shear stress to undrained shear strength. Thus for reinforcement with an embedded plan area A

$$\alpha = T/2(AC_u) \tag{4}$$

Combining equations (2) and (4) leads to a redefinition of the adhesion factor

$$\alpha = (Nc\Sigma a + \beta \Sigma a_s)/(2A) \tag{5}$$

For the specific case of the rod grid under consideration

$$\alpha = (N_c D \Sigma l_n + \beta \pi D \Sigma l_p)/(2A) \tag{6}$$

The above equation was evaluated for the Weldmesh grid using values of 7.5 and 0.5 for N_c and β respectively. This gave rise to a calculated adhesion factor of 0.38, which is very close to the mean measured value of 0.39 (Ingold, 1983). This close agreement is fortuitous. Since the values of the bearing capacity factor and skin adhesion factor are reasonable, it is postulated that the general equations are of the correct form. One omission in equation (5) is the upper limit for the adhesion factor. If consideration is limited to saturated clays, where shear strength is independent of the ambient stress level, then the upper limit of the adhesion factor must be unity, i.e. there will be a critical shear plane discontinuity on both sides of the reinforcement

GRID	APERTURE SIZE (mm)	CELL SIZE (mm)	β (Measured)	α (Theoretical)	α (Measured)
Netlon 1168	5 x 5	6 x 6	0.6	0.88	0.89
Weldmesh 5119	24 x 11	25 x 12	0.5	0.94	1.07

Table 1. Grid data

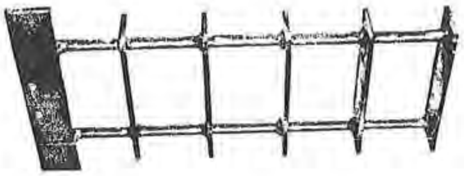

Fig. 1. Special test piece

in the plane of the reinforcement. This thesis was tested using an orthogonal 'grid' whose transverse members were 50 mm deep and 200 mm wide. These transverse members were very stiff, being made from a 6 mm thick steel plate. The two longitudinal members, which were also very stiff, were 12.5 mm diameter steel rods on which the transverse members were attached at 92 mm centres. The general appearance of the test piece including the special pull-out bracket can be seen in Fig. 1. Application of equation (2) indicated an adhesion factor of 2.27. Pull-out tests were conducted together with associated triaxial testing of the clay involved in the tests and resulted in a measured adhesion factor of 0.98.

In the case of an orthogonal grid formed from circular rods of diameter D, a simple analysis can be carried out to assess the relationship between longitudinal and transverse rod spacings, the embedded plan area and the potential adhesion factor. Fig. 2 shows a diagrammatic representation of a single cell of a planar grid with transverse and longitudinal member spacings shown as multiples n_x and n_y, respectively, of the rod diameter.

The hatched area shows the one transverse member and the two halves of the longitudinal members that would react against the pull-out force ΔT. The lagging transverse rod is not included in the grid cell since this forms the leading transverse rod in the adjacent cell. Based on

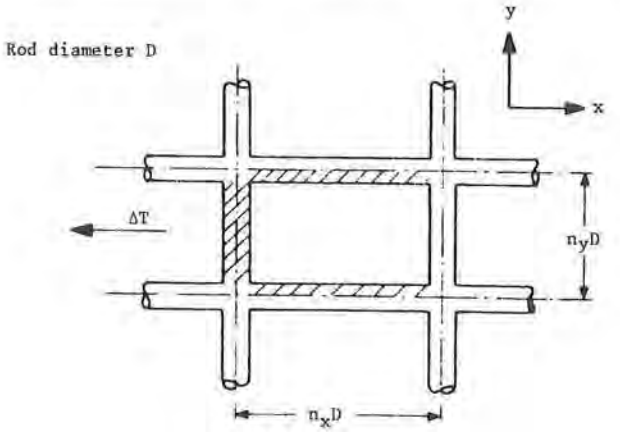

Fig. 2. Geometry of unit grid cell

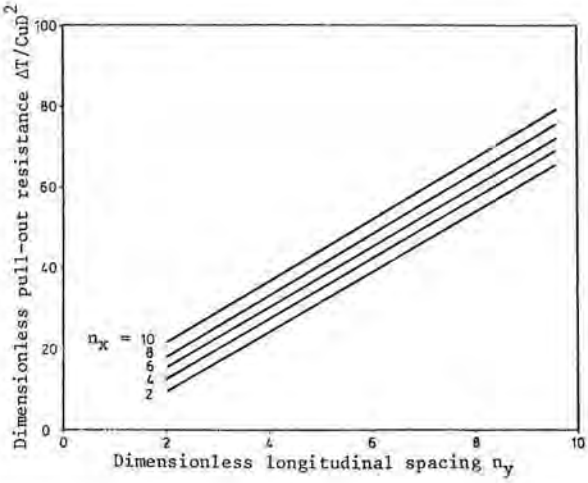

Fig. 3. Variations of $\Delta T/C_uD^2$ with n_x and n_y

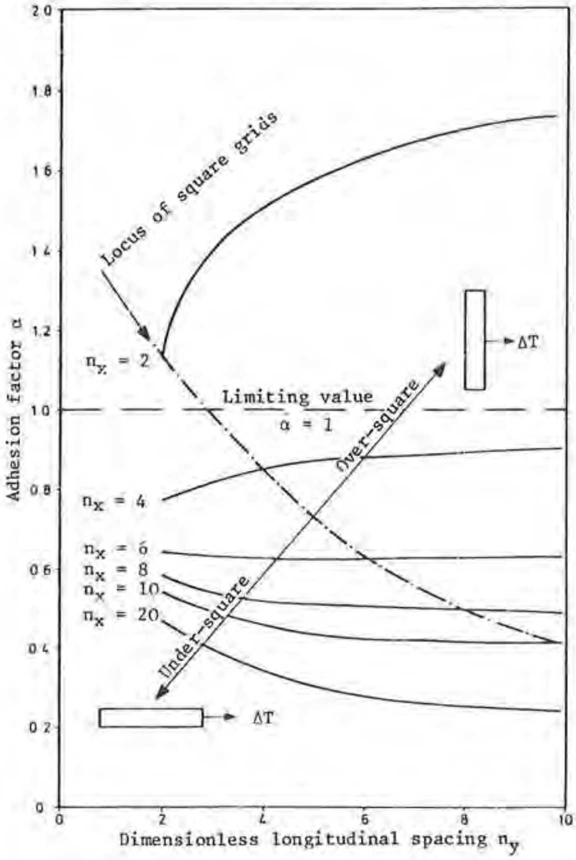

Fig. 4. Variation of adhesion factor with n_x and n_y

this geometry it is possible, using the same argument in deriving equation (3), to obtain an expression for ΔT.

$$\Delta T = N_c C_u D^2(n_y - 1) + \beta C_u \pi D^2(n_x - 1) \tag{7}$$

Obviously ΔT would vary with the square of the rod diameter. However, when equation (7) is rendered dimensionless as shown in equation (8), it becomes apparent that ΔT varies linearly with n_x and n_y.

$$\Delta T/C_u D^2 = N_c(n_y - 1) + \beta\pi(n_x - 1) \tag{8}$$

This variation, which is plotted in Fig. 3 for the previously employed values of $N_c = 7.5$ and $\beta = 0.5$, shows that n_y has a much more significant effect than n_x, since a larger value of n_y is associated with a longer length of the more efficient transverse member per unit cell. A less expected result emerges if the expression for ΔT is substituted into equation (4) together with the plan area of the grid cell $n_x n_y D^2$ to give an expression for the adhesion factor.

$$\alpha = [N_c(n_y - 1) + \beta\pi(n_x - 1)]/(2n_x n_y) \tag{9}$$

The variation of adhesion factor with n_y is plotted in Fig. 4 with a family of curves for n_x. This shows that for low values of n_x, i.e. transverse rods at close centres, the adhesion factor increases with n_y as might be expected. However, since the plan area $n_x n_y D^2$ is also increasing, α levels off. The trend of α increasing with n_y becomes less marked as n_x increases, until at $n_x = 6$ the value of α is almost independent of n_y. For values of $n_x > 6$, the adhesion factor decreases with increasing n_y. This is a function of two things. Firstly, as n_x increases the less efficient longitudinal members, which only generate surface adhesion, are becoming more prominent.

Secondly, as n_y increases the plan area increases and consequently reduces α. The interplay between these factors is quite intriguing. Although a grid with low n_x and high n_y might be thought efficient, its potential pull-out resistance is curtailed by the limiting value of the adhesion factor of unity. Thus, over-square grids ($n_y > n_x$) may not be as efficient as was first thought because of this upper bound limit. It also appears that square grids and under-square grids of high n_y are not efficient. From this theoretical analysis it would appear that an over-square grid with $n_x = 4$ and $n_y > 6$ is most efficient, giving $\alpha = 0.9$. Since α tends to level out for $n_y > 6$, it follows that large n_y, i.e. large transverse rod spacing, might be very economic.

References

Ingold, T. S. (1980). Reinforced clay. PhD thesis, Surrey University.

Ingold, T. S. (1983). A laboratory investigation of grid reinforcements in clay. ASTM Geotechnical Testing Journal, Vol. 6, No. 3, 112-119.

Mr. A. R. Dawson, University of Nottingham

The paper by Jewell et al. (1.3) discussed two types of potential failure mechanism: direct sliding across the top of a grid and pull-out of the grid from between soil. Methods by which load might be transferred between grid and soil were suggested for each mechanism, and these were to some extent confirmed by the slides of stress fields obtained in research work at Oxford with crushed glass.

However, the original work of Jewell's doctoral thesis showed by means of X-ray techniques that a trapezoidal shear zone developed around a small grid inclusion placed at large angles to the plane of shear. Thus a third potential failure mechanism appears to exist at the intersection of grid and shear plane. It may be argued that in a real soil-reinforcement situation the soil-grid interaction local to the shear plane will form an insignificant part of the influence of the whole grid inclusion. However, this remains to be demonstrated.

It is conceivable that this third mechanism is the predominant means by which the soil is strengthened when small randomly-oriented mesh elements are included in the soil as described by Mercer et al. (Paper 8.1).

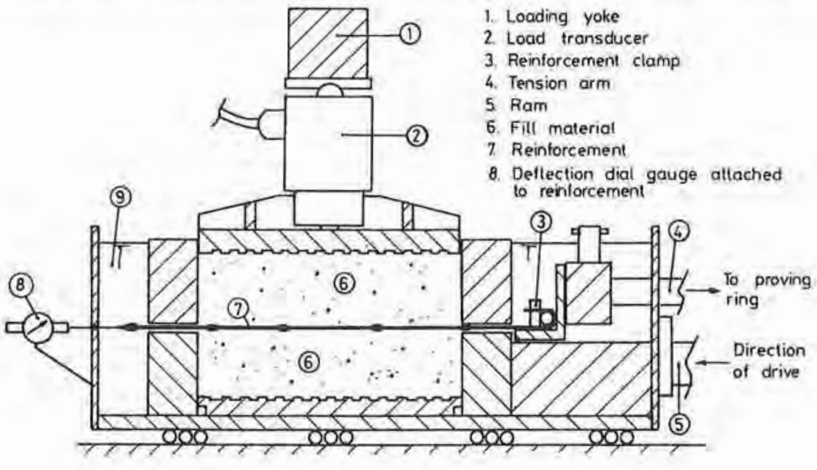

Fig. 5. Modified shear box apparatus

Dr R. W. Sarsby and Mr C. B. Marshall, Bolton Institute of Higher Education

PULL-OUT TESTS ON TENSAR REINFORCEMENT

Introduction

Reinforced Soil is a composite material formed by the addition of relatively inextensible reinforcement to a soil mass so that the inherent low tensile strength of the soil is enhanced in a manner analogous to the use of steel reinforcement in concrete. The amount of 'bond' or friction which is developed between the soil and the reinforcement is thus a very important design parameter.

The interaction between reinforcement and fill is usually determined experimentally using modified direct shear box tests (Schlosser & Juran, 1979) or pull-out tests (Schlosser & Elias, 1978). A method for testing geogrids in direct shear has been developed by Sarsby & Marshall (1983) and the results are presented in paper 1.3 by Jewell et al. Some preliminary pull-out tests have been conducted at Bolton Institute of Higher Education on Tensar geogrid SR2 contained within a medium sand and the results are presented herein.

Apparatus

The apparatus used was a modified direct shear box with a plan area of 300 mm by 300 mm. Both halves of the box were clamped together with spacer pieces between them so that a gap was left in the front and rear faces for the reinforcement to pass through (see Fig. 5). The reinforcement was anchored, via tension arms, to a proving ring and pull-out was achieved by pushing the shear box outwards relative to the reinforcement. To monitor deformation of the reinforcement thin wires were attached to various ribs of the grid. These wires passed out through the rear of the box and were themselves attached to deflection dial gauges.

Normal stress was applied hydraulically to the sample and this was monitored using a load transducer.

Sample preparation and testing

The sand fill was placed and compacted in four equal layers using a vibrating hammer and tamping plate. Each layer was formed by compacting a known weight of soil to a specific thickness to obtain a sample dry density corresponding to 92% of the maximum achievable value. The second layer of the sand was compacted flush with the surface of the bottom half of the shear box and the reinforcement was fed through the gaps in the box and laid flat on the sand. The steel wires were attached to the ribs, after which they were passed out of the box and pulled straight. Two more layers of fill were subsequently placed and compacted.

After the shear box had been mounted in the carriage the reinforcement was attached to the proving ring. The steel wires were tensioned and fastened to the appropriate deflection dial gauges. The requisite normal stress was then applied and the sample was saturated with water.

Samples were sheared (under drained conditions) by driving the shear box outwards at a nominal rate of displacement (relative to the leading edge of the reinforcement) of 0.6 mm/min. Shearing was continued until the limit of travel of the apparatus was reached.

Test data

Details of the tests performed are contained in Table 2.

The stress-strain behaviour of the reinforced samples is presented in Fig. 6 in terms of the equivalent shear stress τ_{mean} acting on each face of the reinforcement and the displacement of the leading edge of the reinforcement, i.e. that part closest to the proving ring, relative to the fill Δ_{mean}. The stress-strain curve for a typical plain sample (test code U3) is included for comparison.

The development of shearing resistance with displacement is very slow and peak resistance is only achieved after large movements. For the

Test Code	Test Type	Normal Stress (kPa)	γ_{dry} (kN/m^3)	$\left(\frac{\gamma_{dry}}{\gamma_{dry\ max}}\right)$ (%)
R1	Reinforced	3	15.7	90
R2	"	15	15.8	91
R3	"	25	15.8	91
R4	"	56	16.1	93
R5	"	75	16.1	93
R6	"	100	15.8	91
U1	Plain	29	15.8	91
U2	"	43	16.0	92
U3	"	80	15.9	91
U4	"	102	16.4	94
U5	"	117	16.0	92

Table 2. Test data

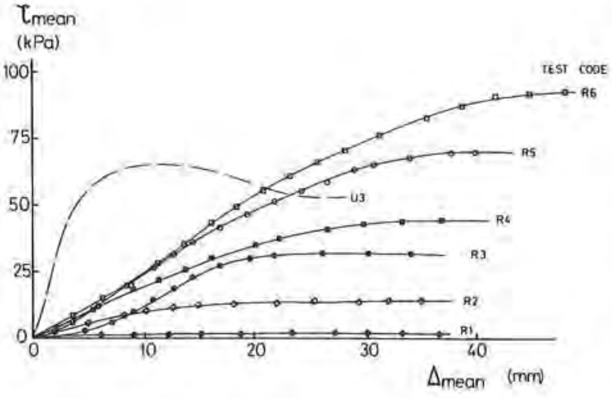

Fig. 6. Stress-strain behaviour

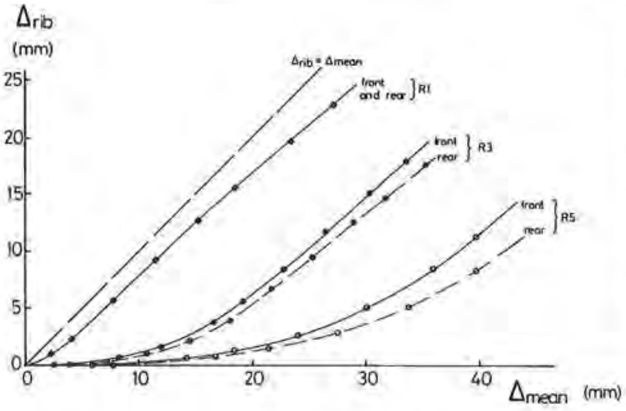

Fig. 7. Reinforcement displacement

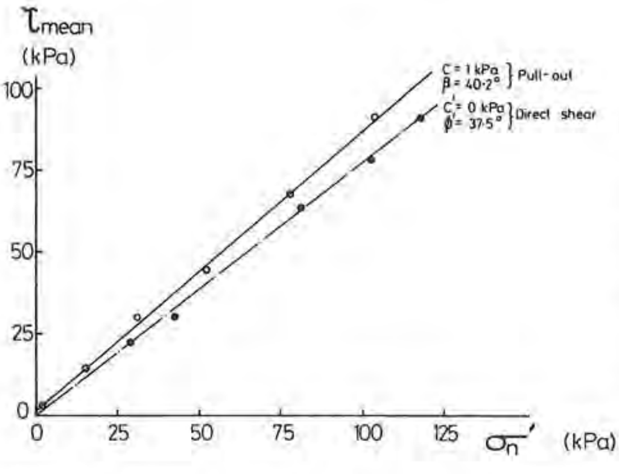

Fig. 8. Effective shear strength parameters

same normal stress the displacement to failure in the pull-out tests was approximately 3.5 times that for soil-on-soil sliding.

At high normal stresses the peak resistance to pull-out was developed only slightly before the limit of travel of the apparatus was reached. However, even at low normal stress levels, there was no marked peak in the stress-strain curves and no significant drop in resistance at large displacements. This is in contrast to the behaviour reported by Alimi et al. (1977) and Jewell (1979) for relatively stiff reinforcements. However, during pull-out of the Tensar grid there was appreciable deformation of the reinforcement, as indicated in Fig. 7. This graph shows the horizontal movement of ribs of the geogrid relative to the movement of the leading edge of the reinforcement for different normal stress levels. The front and rear ribs were approximately 100 mm and 200 mm distant from the leading edge respectively, so that extension of the geogrid can be gauged from the separation of the respective front and rear curves.

In Fig. 8 the peak value of τ_{mean} has been plotted against effective normal stress σ_n'. For the pull-out tests the slope of the resultant line is an equivalent mean shearing angle β, such that $\tan\beta = f_b \tan\phi'$, where f_b is defined in equation (12) of paper 1.3 by Jewell et al. For these pull-out tests the value of f_b is 1.10 as opposed to the theoretical maximum value of unity. This discrepancy is believed to be due to boundary effects in the apparatus, whereby the bearing pressure on some reinforcement ribs is enhanced due to their proximity to the rigid faces of the shear box.

Published data for pull-out tests have indicated values of f_b significantly greater than unity, but it is not certain whether these high values are due to the mechanism of soil-reinforcement interaction or to boundary effects in the testing systems.

It has been proposed in paper 1.3 that the coefficient bond strength f_b can be expressed as

$$f_b = \alpha_S \frac{\tan\delta}{\tan\phi'} + \frac{\sigma_b'}{\sigma_n'}\frac{B}{S}\frac{\alpha_B}{2\tan\phi'}$$

For the sand and reinforcement (Tensar SR2) used, $\phi' = 37.5$ and $\tan\delta = 0.63$. Thus (σ_b'/σ_n') is in the range 15 to 20 approximately and this leads to a predicted f_b in the range 0.82 to 0.93 (as opposed to the measured value of 1.10). Back-analysis of the reinforcement extensions shown in Fig. 7 generates values of 10 to 18 for (σ_b'/σ_n') at peak shearing resistance.

Acknowledgements
The authors wish to acknowledge the patience and dedication of Mr B. Porter and Mr E. Carroll, without whom this work would not have been undertaken.

References
Alimi, I., Bacot, J., Lareal, P., Long, N. T. & Schlosser, F. (1977). Study of adherence between soil and reinforcements. Proc. 9th Int. Conf. Soil Mech., Tokyo.

Fig. 9. Soil wedge on pulled out anchor

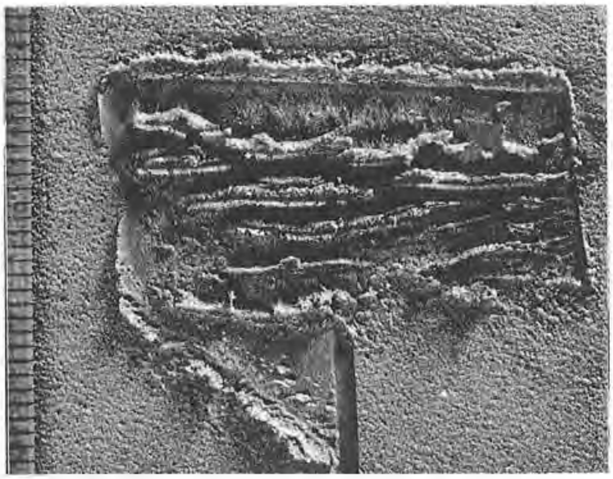

Fig. 11. Tension curl-up on top-split behind the anchor

Fig. 10. Pile-up in front of anchor

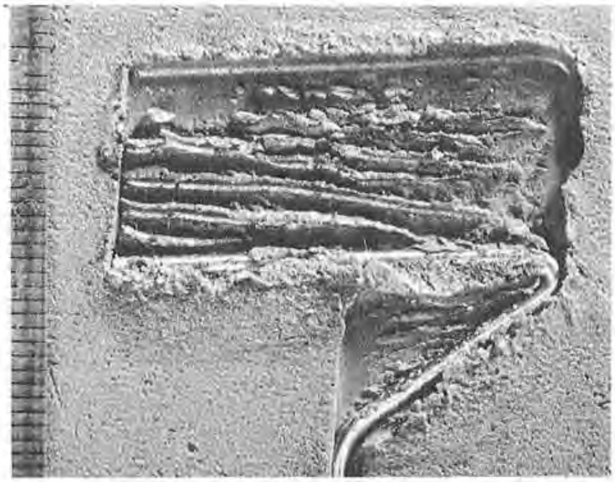

Fig. 12. Tension curl-up on bottom split behind the anchor

Jewell, R. A. (1979). Discussion. Design parameters for artificially improved soils. Proc. 7th Eur. Conf. Soil Mech., Brighton.
Sarsby, R. W. & Marshall, C. B. (1983). A method for determining the interactive behaviour of polymer grids and granular soils. Report No. BCS/G1/2A, Bolton Institute of Higher Education, Bolton.
Schlosser, F. & Elias, V. (1978). Friction in reinforced earth. Symp. on Earth Reinf. ASCE, Pittsburgh.
Schlosser, F. & Juran, I. (1979). General report. Design parameters for artificially improved soils. Proc. 7th Eur. Conf. Soil Mech., Brighton.

Dr R. B. Singh, University of Glasgow
The symposium has highlighted the uses, design methodology, and construction technology pertinent to polymer grids in civil engineering. However, uses of polymer grids are very rare in developing countries and there would appear to be a necessity of cheaper alternatives, or at least of using them in what may be called a 'combined system'. Towards this end the contributor has proposed a system of using TRRL z-type patented anchors (Murray & Irwin, 1981) alternating with embankment situations. The combined system would utilise the advantages of the two systems, viz. reduce the rigidity of a fully anchored earth system and increase the rigidity of a fully reinforced system.

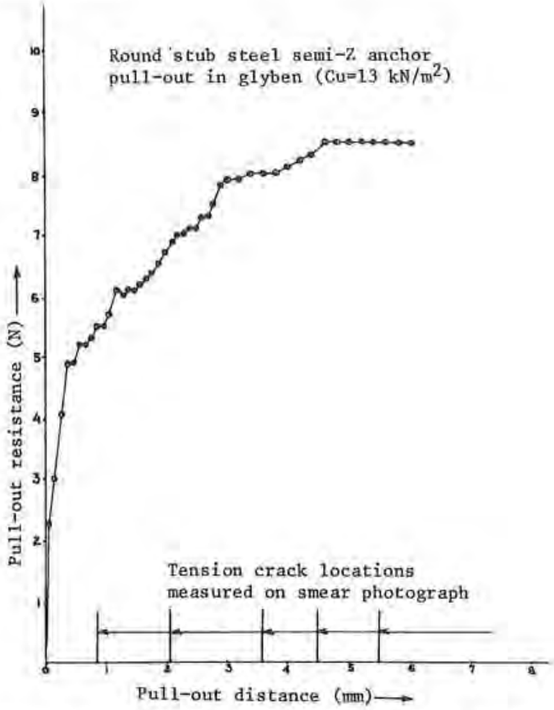

Fig. 13. Pull-out resistance of model anchor versus pull-out distance

More importantly, such a combined system would reduce costs by cutting down on the import cost factor of geogrids. In highly cohesive soils, a suitable filter membrane could possibly be attached to the geogrid layer so that one face of the geogrid would still be available for the soil reinforcement while the other face would promote the dissipation of pore pressures in the plane of the membrane.

With a view to having a better understanding of the failure and resistance mobilisation mechanisms operating in the pull-out of anchors in reinforced soils, the contributor has run small model pull-out tests in a modified direct shear box (inside dimensions 86 mm x 80 mm x 50mm) using an artificially prepared purely cohesive soil called Glyben (Davie & Sutherland, 1977). A special technique of 'split-model' and 'smear traces' which is possible with Glyben has been used. Studies of the soil wedges and pile-ups in front of the pulling out anchors and of tension curl-ups behind the anchor on the smear traces are continuing. It is hoped that the study will eventually help in more exact design formulations of cohesive soils reinforced with anchors. Figs 9-13 present typical information.

References

Murray, R. T. & Irwin, M. J. (1981).
A preliminary study of TRRL anchored earth. TRRL supplementary report 674.

Davie, J. R. & Sutherland, H. B. (1977).
Uplift resistance of cohesive soils. J. Geotech. Div. Am. Soc. Civ. Engrs 103, GT 9, 935-952